UNIVERSIDADE BEIRA INTERIOR

Novel waste-based alkali-activated binders by combining mining and other mineral waste

Naim Sedira

Tese para obtenção do Grau de Doutor em
Engenharia Civil
(3º ciclo de estudos)

Orientador: Prof. Doutor João Paulo de Castro Gomes

Júri:
Prof. Doutor Joaquim Mateus Paulo Serra
Prof.ª Doutora Mirja Illikainen
Prof.ª Doutora Maria Paulina Faria Rodrigues
Prof. Doutor Marcin Górski

4 novembro de 2021

The following grants partially supported the work of this thesis: Doctoral Incentive Grant BID/ICI-FE/Santander Universidades-UBI/2018 financed by the Santander-Totta bank and the University of Beira Interior; Portuguese national funds through FCT – Foundation for Science and Technology, IP, within the research unit C-MADE, Centre of Materials and Building Technologies (CIVE-Central Covilhã-4082), University of Beira Interior, Portugal; and European Commission Horizon 2020 MARIE Skłodowska-CURIE Research and Innovation Staff Exchange Scheme (Grant Agreement Number 645696).

Dedicatory

To the souls of my parents Boulanouar and Naanaa, and of my brother Oussama

Acknowledgements

This thesis could not have been realised without a great deal of guidance and mental and practical support. I would like to thank those people who, during the doctoral program, provided me with everything I needed.

First and foremost, I would like to express my deepest gratitude to my supervisor, Professor Joao Castro-Gomes, for my doctoral program and research's continuous support for his patience, motivation, enthusiasm, and immense knowledge. His excellent guidance helped me in the investigation and writing of this thesis. I am also grateful for his encouragement to present my work at international scientific conferences, allowing me to broaden my horizons. I also express my thanks to Prof. Manuel Magrinho from the Department of Chemistry at the University of Beira Interior for the help to interpret the FT-IR analysis.

I would like to extend my thanks to all the REMINE Project partners for their scientific inputs and support. Moreover, I much appreciate the staff's support at The Civil Engineering and Architecture Department and the R&D unit "Centre for Materials and Building Technologies – C-MADE. Additionally, I acknowledge Dr Ana Paula Gomes of the Optical Centre to support discussions, experiences, and knowledge about XRD and SEM-EDS analysis. I wish to thank all my co-authors in the research project for their contribution to the original articles.

I am also very grateful to the European Commission H2020 programme and Santander Totta Trust for financial support through grants (REMINE Project) and Doctoral scholarships.

Finally, my sincere gratitude to my family for their continuous and unparalleled love, help and support. I am grateful to my sister for always being there for me as a friend. I am forever indebted to my parents and my brother Oussama for giving me the opportunities and experiences that have made me who I am. This journey would not have been possible if not for them, and I dedicate this milestone to their souls.

Abstract

Alkali-activated binders (AABs) are a new kind of binders. AABs can be produced from various industrial waste sources, many of which have remained largely unexplored. Several studies have shown the potential of reusing and valorising mining wastes into alkali-activated binders in the last few years.

In this research, studies on reusing tungsten mining waste mud (TMWM) as a precursor for AABs are carried out. The research provides new insights into enhancing the binding properties and compressive strength of the tungsten mining waste-based alkali-activated binders. Further, it aims studying the microstructure properties of the developed alkali-activated binders. These alkali-activated mixtures were prepared by combining tungsten mining waste mud with other mineral wastes as fine powders. The blended powders included ground red clay brick waste, ground granulated blast furnace slag, electric arc furnace slag and metakaolin. In the research study, the TMWM was taken as the primary precursor for alkali-activation. Other mineral wastes added to the mixtures were considered as complementary precursors added in lower proportions (0, 10, 20, 30, 40, 50 vt.% or wt.%).

The effect of different combinations (TMWM with the other mineral wastes) on the novel binders' characteristics is discussed in depth. The effect of different alkaline activator solutions and liquid/solid ratios is also analysed. The alkali-activated binders' properties studied comprise the following main tests: compressive strength development, microstructure description, reaction products formed, thermal analysis, FT-IR absorbance spectra, porosity determination and pore characterisation. This study's primary focus is the strength development and microstructural properties, as evidence of binding properties of the obtained alkali-activated binders based on TMWM.

In this research, several novel contributions can be listed. The different mineral wastes blended with TMWM were considered to provide an additional source of reactive silica, alumina, and calcium contributing to the formation of more reaction products such as C-S-H, N-A-S-H, C-A-S-H and (N, C)-A-S-H hardened structures. Moreover, adding reactive alumina-silicate rich materials in the blended systems prevents efflorescence phenomena by generating more alkaline activation reaction products. Furthermore, combining TMWM with other mineral wastes reduces the total porosity, the average pore diameter, and the critical pore diameter, resulting in a refinement of the pore structure and an enhancement of the compressive strength development of the alkali-activated binders. Finally, for the

AABs with a low liquid/solid ratio investigated in this research (the blend of TMWM and electric arc furnace slag) a positive correlation between the initial compaction pressure and the compressive strength gain was found. However, regardless of the initial compaction pressure applied, this type of binder can develop significant compressive strength over time.

Keywords

Mining waste, Mineral wastes, Alumina-silicate, Alkaline-activation, Compressive strength, Microstructure, Reaction products.

Resumo

Os ligantes de ativação-alcalina (AABs) são um novo tipo de ligantes, considerados como sendo ligantes de terceira geração, depois da cal e do cimento Portland. Estes podem ser produzidos a partir de várias fontes de resíduos industriais, muitas das quais permanecem praticamente inexploradas. Vários estudos publicados já demonstraram o potencial de reutilização e valorização de resíduos de minas para obtenção de ligantes de ativação-alcalina.

Nesta investigação, são realizados estudos sobre a reutilização de lamas residuais de minas de tungsténio (TMWM) como precursor para AABs. A investigação fornece novos conhecimentos sobre a melhoria das propriedades de ligação e resistência à compressão dos ligantes de ativação alcalina de resíduos de minas de tungsténio. Além disso, visa estudar as propriedades de microestrutura dos aglomerantes alcalinos desenvolvidos. Estas misturas de ativação alcalina foram preparadas combinando lamas de resíduos de minas de tungsténio com outros resíduos minerais em pós finos. Os pós misturados incluem resíduos de tijolo de argila vermelha moída, escória de alto-forno granulada moída, escória de forno de arco elétrico e metacaulino. No estudo de investigação, as TMWM foram tomadas como o precursor primário para a ativação alcalina. Outros resíduos minerais adicionados às misturas foram considerados como precursores complementares, que foram adicionados em proporções inferiores (0, 10, 20, 30, 40, 50 vt.% ou wt.%).

O efeito de diferentes combinações (TMWM com os outros resíduos minerais) nas características dos novos aglutinantes é discutido em profundidade. É também analisado o efeito de diferentes soluções de ativadores alcalinos e rácios líquido/sólido. As propriedades dos ligantes alcalinos estudados compreendem os seguintes testes principais: desenvolvimento da resistência à compressão, descrição da microestrutura, determinação dos produtos de reação formados, análise termogravimétrica, análise de espectros de absorção FT-IR, determinação da porosidade e caracterização da distribuição de poros. O foco principal deste estudo é o desenvolvimento da resistência mecânica e propriedades microestruturais, como evidência das propriedades de aglutinação dos ligantes alcalinos obtidos com base nas TMWM.

Nesta investigação, várias contribuições inovadoras podem ser enumeradas. Os resíduos minerais misturados com TMWM foram considerados para fornecer uma fonte adicional de sílica reativa, alumina, e cálcio, contribuindo para a formação de mais produtos de reação, tais como, estruturas de C-S-H, N-A-S-H, C-A-S-H e (N, C)-A-S-H. Além disso, a adição de

materiais ricos em silicato de alumínio reativo nos sistemas misturados previnem fenómenos de eflorescência, ao gerar mais produtos de reação de ativação alcalina. Além disso, a combinação das TMWM com outros resíduos minerais reduz a porosidade total, o diâmetro médio dos poros, e o diâmetro crítico dos poros, resultando num refinamento da microestrutura e numa melhoria do desenvolvimento da resistência à compressão dos ligantes de ativação alcalina. Finalmente, nos AABs com uma baixa relação líquido/sólido investigados nesta pesquisa (caso mistura de TMWM e escória de forno de arco elétrico) foi encontrada uma correlação positiva entre a pressão inicial de compactação e o ganho de resistência à compressão. Contudo, independentemente da pressão inicial de compactação aplicada, este tipo de ligante pode desenvolver uma resistência compressiva significativa, ao longo do tempo.

Palavras-chave

Resíduos de minas, Resíduos minerais, Alumino-silicatos, Ativação-alcalina, Resistência à compressão, Microestrutura, Produtos de reação.

Original papers

This thesis is based on the following publications, which are referred throughout the text by their Roman numerals:

I. N. Sedira, J. Castro-Gomes, G. Kastiukas, X. Zhou, and A. Vargas, "A review on mineral waste for chemical-activated binders: mineralogical and chemical characteristics," Mining Science., vol. 24, pp. 29–58, 2017. Available from: doi: 10.5277/msc172402

II. N. Sedira, J. Castro-Gomes, and M. Magrinho, "Red clay brick and tungsten mining waste-based alkali-activated binder: Microstructural and mechanical properties," Construction and Building Materials., vol. 190, pp. 1034–1048, 2018. Available from: https://doi.org/10.1016/j.conbuildmat.2018.09.153

III. N. Sedira and J. Castro-gomes, "Effect of activators on hybrid alkaline binder based on tungsten mining waste and ground granulated blast furnace slag," Construction and Building Materials., vol. 232, p. 117176, 2020. Available from: https://doi.org/10.1016/j.conbuildmat.2019.117176

IV. N. Sedira and J. Castro-Gomes, "Alkali-Activated Binders Based on Tungsten Mining Waste and Electric-Arc-Furnace Slag: Compressive Strength and Microstructure Properties," CivilEng, vol. 1, no. 2, pp. 154–180, 2020. Available from: doi:10.3390/civileng1020010

V. N. Sedira and J. Castro-gomes, "Microstructure Features of Ternary Alkali-activated Binder Based on Tungsten Mining Waste, Slag and Metakaolin," KnE Engineering., vol. 5, no. 4, pp. 195–206, 2020. Available from: DOI 10.18502/keg.v5i4.6810

VI. N. Sedira and J. Castro-Gomes, "Low Liquid-to-solid Ratio of Mining Waste and Slag Binary Alkali-activated Material," KnE Engineering., vol. 2020, pp. 202–213, 2020. Available from: DOI 10.18502/keg.v5i5.6941

Contents

List of figures

List of tables

List of abbreviations and acronyms

Materials

AAB	Alkali-activated binder
AABs	Alkali-activated binders
AAMs	Alkali-activated materials
C-A-S-H	Calcium-aluminium-silicate-hydrate
C-S-H	Calcium-silicate-hydrate
EAF-Slag	Electric arc furnace slag
GGBFS	Ground granulated blast furnace slag
HAB	Hybrid alkaline binder
K-A-S-H	Potassium-aluminium-silicate-hydrate
KOH	Potassium hydroxide
MK	Metakaolin
N-A-S-H	Sodium-aluminium-silicate-hydrate
NaOH	Sodium hydroxide
OPC	Ordinary Portland cement
RCBW	Red clay brick waste
S/L	Solid/liquid
SS (Na_2SiO_3)	Sodium silicate
TMWM	Tungsten mining waste mud
WO_3	Tungsten trioxide

Techniques

ATR	Attenuated total reflectance
DTG	Derivative thermogravimetric analysis
EDS	Energy dispersive X-ray
FT-IR	Fourier-transforms infra-red
MIP	Mercury intrusion porosimetry
SEM	Scanning electron microscope
TGA	Thermogravimetric analysis
XRD	X-Ray Diffraction
LOI	Loss on ignition

1. Introduction and aims

1.1. Background

Portland cement is the most widely used material in the construction industry nowadays. However, the cement industry faces challenges related to improving its production processes and reducing the environmental impact generated during the manufacturing of Ordinary Portland Cement (OPC). The Portland cement manufacturing is an energy-intensive process due to limestone combustion at elevated temperatures at around 1450 °C. The Portland cement manufacturing by limestone combustion resulting in significant emissions of several greenhouse gases into the environment. The cement production represents 5-7% of CO_2 emissions worldwide caused mainly by the decarbonisation or decomposition of limestone. For reducing CO_2 emissions and energy consumption, the alkaline activation technology has been extensively studied in the past decades as an alternative binder to Portland cement. The formation of alkali-activated materials uses alkaline activators (such as sodium silicate, sodium hydroxide and potassium hydroxide) to activate precursors (alumina-silicate rich materials, in the form of powders) at room or moderate elevated temperatures. Besides the environmental benefits, AAMs are used as alternative materials with similar, and better physical and mechanical properties to Portland cement [1].

The construction sector industries will benefit by employing waste materials as resource to develop value-added products due to increasing cost and shortage of virgin raw materials. Reuse of industrial by-products to generate value-added products is one of the promising ways to attain green and sustainable development. Alkali-activated materials are essential for construction manufacturing sectors by enabling using waste generated from different sectors, especially those coming from mining activities and industrial (like different types of slags, brick waste, fly ash, and others). The alkaline activation of waste materials is a chemical process that transforms glassy structures (partially or amorphous or metastable) into very compact well-cemented composites [2].

According to the European Union (Eurostat) statistical office, mining and quarrying in Europe generate a high amount of mine tailings, approximately 55% of the total industrial wastes [3]. The mining activity produces an enormous quantity of solid waste materials during mining's lifetime, disposed of in the open air, which causes several environmental issues during waste management. The waste generated from mining and quarrying

industries accumulated in large deposits present a potential risk of environmental pollution and cause severe landscape impacts.
Recent research studies and applications proved alkaline activation as an innovative waste-recovery technology. These recent studies have focused on reusing mineral waste such as red clay brick waste, different mining waste types, ground waste glass and mineral wools. The chemical compositions of this mineral wastes are rich in alumina, silica, and calcium, which are the main needed elements for the alkaline activation technology. Many studies pertinent to recycling waste and the production of eco-friendly binders have been carried out. In those, a promising alternative for mining waste management appears to be alkaline activation to produce secondary materials [4]. Different mine tailings from various mining operations around the world have been investigated regarding their potential for alkaline activation [5–8].

The Panasqueira mine is located in the Central Iberian Zone of the Palaeozoic Iberian Massif in Portugal, which is one of the most important metallogenic provinces of Europe. Panasqueira is one of the largest operating tungsten mines in the Market Economy Countries and is considered a world-class Tungsten-Tin-Copper vein-type deposit. The tungsten concentrates have a Tungsten trioxide (WO_3) content of 74 – 75%, one of the highest grades available in the market. The Panasqueira mine mines an iron-rich tungstate termed ferberite. Currently about 85,000 - 95,000 MTU (1 MTU - metric tonne unit - is equal to 10 kg) of the WO_3 concentrate generated annually [9]. During the production process of the principal metal of tungsten and by-products of copper, silver and tin, a significant amount of wastes is also generated. In Panasqueira mine, three categories of wastes are generated and classified as follow: the mining activities and the hydro cyclone heavy media separation generates contaminated water containing arsenic, phosphorus, tin and copper. Quartz and schist come from the ore's crushing, and the tailings (tungsten mining waste mud) are received from the water-treatment plant.

Tungsten mining waste mud is a mine tailing leftover from the ore processing conveyed and stored as a slurry in the dump area. The mining waste mud dump poses an environmental risk, by causing contamination of the soil, pollution of the water and air in the surrounding areas [10]. The tungsten processing industries lead to possible adverse health effects for humans because tungsten and some of its compounds have low solubility [11]. According to Castro-Gomes et al. [12], the mineralogy of tailings from Panasqueira tungsten mining waste was found to be mainly quartz and muscovite. TMWM have shown the possibility of being a precursor to produce alkali-activated materials. Pacheco-Torgal et al. [13], in their initial study, reused TMWM as a precursor in the alkaline activation by subjecting the

precursor (TMWM) to a thermal treatment at 950°C for two hours. The calcinated TMWM was mixed with (Sodium Hydroxide and Sodium Silicate) solutions and minor quantities of calcium hydroxide. In their study they obtained alkali-activated concrete. It was a mixture of limestone aggregates and the alkali-activated binder (aggregate/binder ratio =1.5). In turn, the alkali-activated binder consisted of a mix of the precursor and 10 % of calcium hydroxide ($Ca(OH)_2$) combined with sodium hydroxide solution (NaOH 20 M). For this combination, the resulted alkali-activated concrete reached a compressive strength of $fc_{(56)}$ = 65.3 MPa at 56 days of curing.

The present thesis has been conducted to reuse TMWM in its natural state (without calcination), by blending TMWM with other alumina-silicate rich materials, such as metakaolin and other mineral wastes (red clay brick waste, blast furnace slag and ground waste glass). It aimed to improve the compressive strength and the microstructure properties of the tungsten mining waste-based alkali-activated binder system.

To improve the compressive strength and the microstructure properties of tungsten mining waste-based alkali-activated binder, the (TMWM) precursor was first blended in various proportion with (RCBW). The investigation conducted with red clay brick waste is presented in **Paper II**. In the literature, RCBW was used as a precursor to making alkali-activated binder. The binder prepared by RCBW generating an excellent compressive strength and microstructure properties, due to its chemical and mineralogical composition. The blend of RCBW with TMWM increases the compressive strength results, generates more reaction products, and enhances the binder's porosity and pore structure.

Paper III investigated the effect of different combinations of alkaline activator solutions, the activators' concentration (sodium hydroxide and potassium hydroxide), and the solid/liquid ratio on the binder's properties. The precursors in the study were 90 vt. % TMWM blended with 10 vt. % GGBFS; the use of 10 vt. % of GGBFS was to incorporate Ca into the mixtures. In this study, different types of alkaline activators were used. One of the binders developed in **Paper III** used an alkaline activator solution containing more soluble silicate. The alkaline activator solutions were prepared by dissolving glass waste into NaOH. The objective was to add more alkali metal silicates, which play an important role in the polymerisation reaction [14]. The alkaline activator potassium hydroxide has shown good results.

The blend of TMWM and EAF-Slag was studied in **Paper IV.** These precursors were blended in different ratios and mixed with the activator solution (SS+ Potassium hydroxide)

to get TMWM-EAF-Slag alkali-activated binders. The study was conducted to determine the effect of different dosages of EAF-Slag on the compressive strength, reaction products, porosity, and pore structure of the TMWM-EAF-Slag alkali-activated binders.

In **Paper V** the TMWM was mixed with a minor proportion of GGBFS and MK; 10 wt.% of each precursor. Since GGBFS is a calcium-rich material it was incorporated into the admixtures to increase its calcium content, while MK was the alumina-silicate-rich source material. These precursors (MK and GGBFS) were used to yield silicon, calcium, and aluminium for the alkaline activation reaction.

The study in **Paper VI** was focused on decreasing the content of the activator solution in the system by reducing the liquid/solid ratio. For this purpose, samples of TMWM and EAF-Slag were submitted to different pressure compaction before activation. The combination between the low liquid/solid (L/S) ratio and compaction pressure enhances the compressive strength and the resulting binders' microstructure properties.

In **Papers IV** and **V**, the different reaction products formed in the tungsten mining waste-based alkali-activated binder were studied. The main reaction products developed in the binder after the alkaline activation are C-S-H and N-A-S-H hardened structures. The presence of needles found in the scanning electron microscopy (SEM) images of tungsten mining waste-based alkali-activated binder after the alkaline activation may correspond to the formation of natrite (Na_2CO_3) needles due to the low reactivity of TMWM, where Na in the mixture remained unreactive. During the curing time, the Na reacted with the CO_2 in the atmosphere and formed Na_2CO_3, causing the efflorescence phenomena. As expected, the presence of unreacted potassium (in a system with K as an activator) under the efflorescence phenomena may form potassium carbonate (K_2CO_3) [15].

1.2. Approach and aims of the thesis

This investigation aims to complement the knowledge in the reusing and valorising mining waste and other industrial wastes by alkaline activation in a general context. Furthermore, it aims developing a new category of alkali-activated materials based mainly on mining waste and industrial wastes instead of Portland cement-based binders.

The research was mainly focused on enhancing the compressive strength results and studying the tungsten mining waste-based alkali-activated binders' microstructure properties by combining mining waste with other mineral wastes. The objective of the

research was to improve the properties (microstructure and compressive strength) of TMWM-AABs; for this, in all the studies conducted in this research, the TMWM powder was the primary precursor blended with other mineral wastes in minor proportion (other wastes content were 0, 10, 20, 30, 40, 50 vt.% or wt.%).

The general target of this research was to enhance the reactivity of TMWM without calcination. It was also targeted to improve the tungsten mining waste-based alkali-activated materials' different properties by blending TMWM blended with various mineral waste (RCBW, GGBFS, EAF-Slag) and also with a minor proportion of alumina-silicate source material (MK).

The individual objectives of the research are the following:

1. To develop a new alkali-activated binder based on tungsten mining waste mud blended with other different alumina-silicate rich materials and by-product wastes.

2. Develop a new hybrid alkaline binder based on tungsten mining waste blended with granulated grounded blast furnace slag using different alkaline activator solutions.

3. To research the possibility of enhancing the binders' compressive strengths and improving the binders' durability by decreasing the total porosity and pore size distribution.

4. Study the different reaction products generated when TMWM was partially replaced by other by-product wastes or alumina-silicate source materials.

5. To control the formation of efflorescence (white crystalline sodium carbonate) in the tungsten mining waste-based alkali-activated binders by improving the mix design. The efflorescence may be accompanied by further degradation of the alkali-activated binders.

Prior to the laboratory research carried on this thesis, a literature review on alkali-activated materials state-of-the-art was carried on, as presented in **Paper I**. This review was essential to better understand the research gaps needed to be studied, in particularly, the approach on combining wastes with complementary chemical elements and reactive potential, for enhancing waste-based alkali activated binders.

The alkaline activation of tungsten mining waste mud was studied in **Papers II, III, IV, V** and **VI**. In Paper **II** being on the alkaline activation of TMWM blended with RCBW, the study investigated the effect of RCBW dosages that replaced the TMWM in the mixtures on the compressive strength and the microstructure properties of the resulted binders. Simultaneously, the impact of various alkaline activator solutions on the compressive strength and the microstructure properties of the hybrid alkaline binders produced based

on tungsten mining waste mud and ground granulated blast furnace slag which was investigated in **Paper III**.

In **Paper IV** and **VI,** the tungsten mining waste mud was blended with electric arc furnace slag in various proportions, where the EAF-Slag was partially replaced the TMWM in the AABs mixtures with variable dosages in **Paper IV**, to improve the performance of the tungsten mining waste mud and electric arc furnace slag-based alkali-activated binders. However, in **Paper VI,** the ratio of the precursors TMWM/EAF-Slag was fixed as 50-50 wt. % and the compacting pressures were increasing from 20 MPa to 100 MPa.

1.3. Outline of the thesis

This thesis is organised into 5 chapters. The **1st Chapter** provides an introduction to the topic. The **2nd Chapter** describes the state-of-the-art, which reviews the literature on alkali-activated materials, the history of alkali activation as cementitious material, and the recent advances in the development of binders obtained from mineral wastes. It lists the mineral waste that can be used to produce alkali-activated binders, and the reaction products of alkali-activated binders. Besides, it described the chemical activators that can be effectively utilised in the alkaline activation technology. The materials and methods used in this work are introduced in the **3rd Chapter**. The results and Discussion are presented in the **4th Chapter**. Finally, the conclusions to be drawn from the research and recommendations for further research are set out in the **5th Chapter**

2.State-of-the-art

2.1. Mining waste

The mining industry produces large amounts of solid waste which is composed of coarse aggregates or fine particles. In 2010, the mining industry was the world's largest waste producer with 65 billion tons of waste rock and 14 billion tons of mining tailings [16]. The European mining industry is responsible for 55% of mining total industrial wastes [3], where about 4.9% is incinerated, 43% is recovered, and 51% is adequately landfilled of all the generated mining waste [17]. The generated mining waste has different chemical and physical properties depending on the mined ore's mineralogy and the methods used to produce valuable metals [18].

To promote sustainability practices in the mining industry, various mining wastes have been used as source materials to make alkali-activated materials as shown in Fig. 1. The major mining wastes currently studied and reused as a precursor for alkali-activated materials are red mud; tungsten mining waste and kaolin mining waste [19]. For example, Demir and Derun have used Gold mine tailings as precursor blended with Al_2O_3 as an additive due to low Al_2O_3 content of gold mine tailings. The precursor was mixed with the alkaline activator solutions (sodium hydroxide and sodium silicate) to make an alkali-activated binder. The study shows positive results regarding reusing mining waste as a raw material for the alkaline activation-synthesis. Moreover, the optimum alkali-activated binder sample shows a positive adsorption efficiency [20].

2.1.1. Tungsten mining waste

Tungsten mining waste mud is a mine tailing leftover from the ore processing conveyed and stored as a slurry in the dump area. The mining waste mud dump poses an environmental risk, by causing contamination of the soil, pollution of the water and air in the surrounding areas [10]. The tungsten processing industries lead to possible adverse health effects for humans because tungsten and some of its compounds have low solubility [11]. Tungsten mining wastes work very well as complementary precursors in alkali activated cement, mainly when this cement is used for pH buffering, due to its high alkalinity. Furthermore, the high alkalinity of this type of waste slightly increases the intrinsic alkalinity of the reactions. When used together with other more reactive wastes, it enhances the dissolution of ionic species and generating higher binding gel volumes [19]. The earliest use of mining waste mud as a precursor for the alkaline activation was preliminarily investigated by

Pacheco-Torgal et al., in 2005 [21]. The mining waste mud was subjected to heat treatment to achieve the dehydroxylated state. In 2007 and by subjecting the precursor (TMWM) to a thermal treatment at 950°C for 2 h, the calcinated TMWM was mixed with alkaline activators (Sodium Hydroxide and Sodium Silicate) solution and minor quantities of calcium hydroxide. In their study they obtained and alkaline activated binder and concrete. The alkali-activated concrete was produced with limestone aggregates (aggregate/binder ratio =1.5). In turn, the alkali-activated binder consisted of a mix of the precursor and 10 % of calcium hydroxide ($Ca(OH)_2$) with sodium hydroxide solution (NaOH 20 M). For this combination, the resulted alkali-activated concrete reached a compressive strength of $fc_{(56)}$ = 65.3 MPa at 56 days of curing [13].

Fig. 1. Reusing of mining waste into alkali-activated binder - circular approach

Later, G. Kastiukas et al. [22] replaced 40 wt.% of tungsten mining waste mud with waste ground glass, to improve tungsten mining properties waste-based alkali-activated binder, They used sodium silicate with sodium hydroxide as alkaline activator solution. The study has shown that the addition of waste glass to the mixtures was a very sustainable and practical method of improving TMWM degree of amorphic without calcination treatments of TMWM. Where up to 40 wt.% of waste glass, with a mean particle size of 39.6 μm, it can

be successfully blended with TMWM to increase the amorphous nature of the binary blend by 21%. In other investigation, G. Kastiukas and X. Zhou successfully blended tungsten mining waste mud with ground waste glass and cured the alkali-activated paste primarily at room temperature and evaluated it to have a low activating solution demand. After the cure for 28-day, the AAB's compressive strength result was above 42 MPa when an activator/precursor ratio was maintained < 0.28 [23].

2.2. Alkali-activated materials

Alkali-activated materials are known as potential alternatives to OPC to limit CO_2 emissions and beneficiate several mineral wastes into useful products. Nowadays, there is broad global research and industrial interest in alkali-activated materials as ecologically and technically suitable binders [24]. The alkaline activation of aluminosilicate minerals and industrial by-products has been a considerable study topic over the past decades. Such alkali-activated binders are produced by a chemical reaction between an alumina-silicate precursor (solid powder) and an alkaline activator (solution) to form a hardened stable system. Furthermore, AABs demonstrate similar engineering properties to ordinary Portland cement (OPC) mixtures and may even have a lower CO_2 footprint than their performance equivalent ordinary Portland cement formulations. However, the properties of AABs vary significantly depending on the nature of solid precursor powders (e.g. mining wastes, RCBW, fly ash, metakaolin, slags, etc.), their reactivity, and the alkaline activator used (e.g. NaOH, KOH and/or Na_2SiO_3), which in turn alters the balances of product phases formed in the alkali-activated materials in the hardened state [25].

The development of alkali-activated materials can be traced back recently to the beginning of the last century. **Paper I** give a brief outlook of the historical background about the essential events in developing the alkali-activated materials. The German chemist Kühl was the first one who uses alkalis as a component in cement-based materials and publishes work related to alkali-activated materials back to 1908 [26]. He studied the setting of basic blast furnace slag blended with potassium hydroxide solution (KOH). Since then, many studies have been conducted to analyse the role of alkalis plays in cementitious systems. However, only decades later did this type of cementitious material receive significant attention. The investigations undertaken by Feret (1939) and Purdon (1940) were considered the earliest studies on activated slag. In 1940 the first milestone happened, when a detailed study published by the British chemist Purdon about the clinker free cement consisting of slag and sodium hydroxide [27], later turning them into a commercial product under the name 'Purdocement'. Structures built in the 1950s using Purdocement still exist and have been

surveyed in a recent publication in 2015 by Buchwald et al. [28], concluding that the structures were even fit for the purpose their respective service life.

The main research progress in alkaline activation technology for the next several decades came from a Ukrainian research group initially led by Glukhovsky and later by Krivenko. Although not until 1959 an important breakthrough was made by Glukhovsky using reactive alumino-silicates source materials, and alkalis metal solutions to be understanding and development of binders. Glukhovsky published work about the theoretical basis of alkaline cement called "soil silicates". However, there was a substantial difference between the "soil silicates", and a previous study by Krivenko in 1994, as the alkali in soil silicates acts as a structure-forming element. Through the efforts of Glukhovsky and Krivenko, they developed alkali-activated mixes based on a wide range of precursor and activator chemistries, including both low and high calcium binder systems. The alkali-activated materials were adopted in a wide range of applications [29]. Further, Krivenko categorised the alkaline cement depending on the starting materials into two groups. The first group is the alkaline binding system Me_2O-Me_2O_3-SiO_2-H_2O, and the second group is the alkaline-alkali earth system Me_2O-MeO-Me_2O_3-SiO_2- H_2O.

The next few years have seen exponential growth in research, by the 1970s, following a series of frequent fires in France, the scientists had to develop a material that was able to resist such attack, the French scientist and engineer Prof. Joseph Davidovits developed a class of solid materials similar to the alkaline binding system, using sintering products of kaolinite and limestone or dolomite as the alumina-silicate constituents. In 1991 Davidovits adopted the term "Geopolymer" for various alkali-alumina-silicate binder systems and is now widely recognised as a generic term for alkali-activated binder systems. Geopolymers also generated some trademarks, the most famous one was Pyrament, but alkali-activated binders have begun to acquire real technological significance in later ages. In 1999 Palomo et al. [2], published the first article under the title: "Alkali-activated fly ashes: A cement for the future", investigating the possibility of producing new cement using fly ash the waste generating from coal-fired power plants. From nearly 2000 until now, key researchers such as Palomo, Van Van Deventer, Roy and Provis made some fundamental and systematic studies, and provide a more fundamental science base to this technology. C. Shi in conjunction with P. Krivenko and D. Roy in 2006 published the first book which reviewed and summarised worldwide research advances in alkali-activated cement and concrete. Therefore, in 2014 J. Provis and J.Van Deventer, presented a state-of-the art report about AAMs. The report had been prepared by the RILEM Technical Committee on Alkali-

Activated Materials (TC 224-AAM). Now the alkaline activation technology is well accepted from science, but still not widely accepted in the industry.

2.3. Alkaline activator solutions

The alkaline activation process requires chemical alkaline activators, at least one, to initiate the reaction. In general, alkali silicates and hydroxides at high pH values, are needed to start the dissolution phase. Sodium hydroxide (NaOH) and sodium silicate ($nSiO_2Na_2O$) are the most frequent activators used individually or as a solution mixture. However, potassium hydroxide (KOH) and potassium water glass ($nSiO_2K_2O$) are also used to some extent [14]. The different types of alkaline activators and their use in alkaline activation technology are briefly described in the literature review **Paper I**.

2.4. Reaction products of alkali-activated materials

The reaction, structure and properties of the AAMs are controlled by several factors, including the chemical composition and the nature of the alumina-silicate source materials, the types and concentrations of the alkaline activator solutions and curing conditions. In the alkaline activation, two kinds of alkali-activated binders' reaction mechanism can be established [2]. The first mechanism involves the alkaline activation of precursors with low-calcium (calcium-free raw materials) like metakaolin using a medium to high alkaline activator solutions, leading to a polymeric network formation of sodium alumina-silicate hydrates (N-A-S-H) phases as reaction products. The second system involves the alkaline activation of calcium-rich precursors like granulated grounded blast furnace slags, with a high content of Ca atoms. This precursor's alkaline activation is realised using moderate alkaline solutions leading to calcium silicate hydrates (C-S-H) gel with a lower Ca/Si ratio, and calcium alumina-silicate hydrates (C-A-S-H) phases as reaction products. The resulted alkali-activated binders generated high mechanical strength similar to ordinary Portland cement.

Many investigations conducted in the microstructural understanding of AAMs focus on reaction product phases compatibility and phase compositions in the blended alkali-activated systems. In the alkaline activation of composite systems like TMWM/Slag, the raw materials composition plays a more complex role. It is difficult to determine the exact phases formed because of the systems' high chemical complexity due to varying parameters like the precursor's chemical compositions, the alkaline activating solutions, and the used liquid/solid ratio. The alkaline activation of blended precursor contains low calcium

alumina-silicates; the reaction leads to form sodium alumina-silicate hydrates (N-A-S-H) gels. While the precursor has calcium-rich alumina-silicates leads to the formation of calcium alumina-silicate hydrate (C-A-S-H) gels. In the blended precursor systems, both coexistence and interactions occur between C-A-S-H and N-A-S-H type gels [30]. Both typical reaction product phases can form simultaneously within one blended precursor system [31]; the presence of calcium leads to the formation of C-A-S-H type gels and destroys the N-A-S-H gel structure to some degree by partially replacing sodium with calcium to form (N,C)-A-S-H gels [32]. Simultaneously, the increased availability of aluminates strongly influences the calcium silicate hydrates (C-S-H) gel composition and structure [33]. Also, a higher degree of crosslinking within the reaction products is achieved [34]. The alkaline activation of low calcium alumina-silicates leads to the formation of so-called N-A-S-H gels. Furthermore, in high pH conditions, aqueous aluminate and aqueous calcium modify N-A-S-H gels leading to the partial substitution of sodium with calcium to form (N,C)-A-S-H gels [35]. Different precursors' silicate may exhibit different depolymerisation rates and availability under various conditions such as curing temperature and alkaline activator solution concentration.

2.5. Advances in binder development: non-conventional mineral wastes

An alkaline activation is an approach for the non-fired or low-temperature cement production from various natural and technogenic alumina-silicate materials, whose properties are comparable to Portland cement. Recently alkaline activation technology has gained increasing appeal from the standpoints of theoretical research and practical development. Progress in this area has also been derived from a constant expansion of the raw materials base, the possibility of using a wide range of natural and reusing of waste alumina-silicate rich source materials, and ways to improve the different performances of AAMs through the introduction of mineral additions and chemical additives including various fibres [36]. An extensive range of mostly low value or waste materials can be valorised and reused to produce cementitious materials using alkaline activation technology. More recently, however, research studies and applications of alkali-activated materials have become more innovative with the types of raw materials used for alkaline activation and have demonstrated the potential of using more non-conventional materials such as mining waste, waste grounded glass, incineration products obtained from sewage sludge, and mineral wools. The chemical composition of novel precursors used in the production of alkali-activated materials is rich in alumina or silicates, which are the main

compounds in such type of materials. Researchers also study the methods of the alkaline activation of each and their availability.

Large quantities of waste resulting during the production process are disposed of in the open air causing a severe environmental impact. Thus, their investigation about how to reuse this type of waste in the building and construction industry is required. The availability and predominant elements of essential waste materials, and the physical characteristics of novel precursors and the materials derived from them are described in **Paper I**. These novel precursors are ordered in terms of the amount generated (from the highest to the lowest quantity) as it shows in Table 1.

2.5.1. Alkali-activated of combining industrial wastes

Blending calcium-rich materials with low-calcium raw materials has become an increasingly relevant research area for alkaline activation technology. Using reactive calcium-rich sources provides a balance between strength and durability. The blending of calcium-rich materials and alumina-silicate waste materials with low reactivity may reuse this waste and produce an alkali-activated material with high properties. In 2015 Rakhimova and Rakhimov investigated the influence of several variables on the production of alkali-activated materials made from ground granulated blast furnace slag (GGBFS) and different red clay brick waste types. Their study sought to explore the influence of blending two other waste materials, in varying percentages, on the final characteristics of alkali-activated materials. They also experimented with the concentration and type of alkaline activator solution, and the curing condition and time. This study offers an excellent overview of the complex variables that drive alkali-activated cement development. The research shows that the strength characteristics of the alkali-activated material are dependent firstly on the type of alkaline activator solution, secondly by the dosages of red clay brick added to the admixtures, followed by the precursors grinding method, curing method, and, lastly, on the chemical and mineralogical composition and origin of the red clay brick used [37].

Table 1. Alkali-activated materials from novel precursors versus availability, main chemical composition and provenance/country.

Types of waste			***Process of production***	***Amount generated (tonnes/year)***	***Predominant elements (%)***	***Mineralogy***	***Provenance/Country***	***Sources***
Mineral Processing tailings	Coal gangue		Excavation and washing of the coal mine	2×10^{11}	SiO_2 (39,08)	Predominantly crystalline	China	[38]
	Red mud		Residue of alumina production process (Bayer process)	120×10^6	Fe_2O_3 (30.9)	Predominantly amorphous	Worldwide	[39]
	Mine tailings	Iron Ore	Waste from Iron ore mine tailings production	632×10^6	SiO_2 (57.31)	(*)	Western Australia	[40]
		Copper	The mining and processing of copper	0.58×10^6	(*)	(*)	Kilembe area (Western Uganda)	[41]
		Tungsten	Mineral extraction and processing produce	0.37×10	SiO_2 (53.48)	Predominantly crystalline	Panasqueira/ Portugal	[42]
		Chromite Ore	The high lime process	0.06×10^6	CaO (34.27)	Predominantly amorphous	China	[43]
		Vanadium	Tailing of vanadium extraction from stone coal	extracting 1 tonne of V_2O_5 generates 120–150 tonnes of tailing	SiO_2 (64.17)	Predominantly crystalline	China	[44]
Incinerator bottom ash (IBA)			Incineration municipal solid waste	10^{12}	(*)	(*)	Taiwan	[45]
Waste glass			Disposed solid waste	14×10^6	SiO_2 (60-80)	Amorphous	Worldwide	[46]
Palm oil fuel ash			Cooking and food processing	10×10^6	SiO_2 (61.33)	Predominantly crystalline	Malaysia	[47]
Coffee waste			Treatment of coffee powders with hot water	6×10^6	(*)	(*)	worldwide	[48]
Incineration products of sludges	Wastepaper sludge		Effluent treatment processes	4.5×10^6	TiO_2 (13.2)	(*)	Europe	[49]
	Sludges resulting from WT		Waste by-product from the water treatment process	11×10^4 tons/wet S 25.6×10^4 tons/ sec	SiO_2 (58.99)	(*)	Thailand	[50]
Mineral wools	Rock		Produced at high temperatures by melting quartz sand, basalt)	2.3×10^6	SiO_2(62.4)	Amorphous	Worldwide	[51]
	Glass				SiO_2(40.4)	Amorphous		
Fluid catalytic cracking			Petroleum refining processes	0.2×10^6	Al_2O_3 (48.40)	Semi-Crystalline	Worldwide	[52]
Rice husk bark ash			Biomass power plants	0.16×10^6	SiO_2 (81.36)	Amorphous	The power Plant company providing RHBA	[53]
Silico-manganese (SiMn) slag			Electric arc furnace technology	0.15×10^6	SiO_2 (42,6)	Crystalline	Spain	[54]
Ceramic waste	Red clay brick		Industry and the construction sector	3-7 % by weight of total Production.	SiO_2(50.9)	(*)	European ceramic industry.	[55]
	Porcelain				SiO_2(71.3)	(*)		

(*) Not provided by the authors

2.5.2. Upcycling mining waste and other industrial waste by alkaline activation

The recycling and reuse of mining wastes is, therefore, a significant environmental challenge. At the same time, the low reactivity of mining waste mud decreases its recycling capacity into alkali-activated materials. Many researchers have utilised poorly reactive mine tailings as raw materials with reactive co-binder (mainly metakaolin or blast furnace slag) in alkali activation. Additionally, the reactivity of the mine tailings can be improved by different treatments [56]. However, other researchers were using the mining waste without treatment but combined with other mineral wastes such as the study conducted by J. Kiventerä et al. [5], to investigate the possibility of immobilising several heavy metals from gold mine tailings by alkaline activation. Their research blended 40-50 wt% gold mine tailings with metakaolin and blast furnace slag as precursor mixed with alkaline activator solution (sodium hydroxide and sodium silicate). The resulted alkali-activated samples were cured at room temperature. They found out that various elements (Cr, Cu, Ni, Zn and Mn) from gold mine tailings can immobilise almost completely by alkaline activation with a suitable co-binder material. The immobilisation efficiency was highly improved with more extended curing period also for the problematic elements As, V, Sb and B. Moreover, by investigating the influence of alkaline activator solution and blend proportions they developed an alkali-activated binder from a blend of sulphidic mine tailings and GGBFS. By experimenting with the sodium hydroxide (NaOH) concentration and GGBFS content, the alkali-activated binder's compressive strength was increased from 1.8 to 25 MPa when 25 wt.% of sulphidic tailings from gold mine was replaced by GGBFS. This study demonstrated that good mechanical properties could be obtained from the alkali-activated binders produced by blending mine tailings and GGBFS; however, the environmental consequences need to be studied to determine whether the mine tailings can be immobilised in the geopolymer.

Other studies that have conducted leachate analyses have shown some promising results in this area [6]. H. Paiva et al. [57] studied the feasibility of reusing high sulfidic tailings as a raw material in the manufacture of alkali-activated materials. The mine tailing was used as a fine aggregate along with metakaolin and blast furnace slag as a precursor, to investigate the effects of the precursor type, the influence of the dosages of mine tailing added to the admixtures, the impact of temperature and curing conditions. They found that the high sulfidic tailings did not react due to its composition; however, the blended high sulfidic tailings and metakaolin generated better compressive strength results (>20MPa) and a faster reactive nature compared to the binder prepared with blended blast furnace slag and high sulfidic mine tailing. Jiao et al. [58] used vanadium mining tailings blended with

metakaolin as an aluminium source using solid sodium hydroxide for the alkaline activation-synthesis. Results showed that adding 30% of metakaolin to vanadium mining tailings improved the compressive strength and formed more reaction product phases. The compressive strength of the binder achieved 55.7 MPa after 7 days of curing. In another study, vanadium mine tailings were blended with fly ash as precursors and solid sodium silicate as an alkaline activator to produce an alkali-activated binder. The paste was cured at room temperature (28 °C). These authors suggested that the vanadium tailings possessed the potential to synthesise fire-resistant alkali-activated products [44].

3.Materials and methods

3.1. Materials

3.1.1. Precursors

The precursors used in this research were based on tungsten mining waste mud as the primary precursor blended, with different percentual ratios, with other waste by-products: namely, red clay brick, granulated grounded blast furnace slag or electric arc furnace slag, or with alumina-silicate rich material (Metakaolin). The steps followed to reuse and valorise the other wastes to be used as precursors for the alkaline activation are described in Fig. 2.

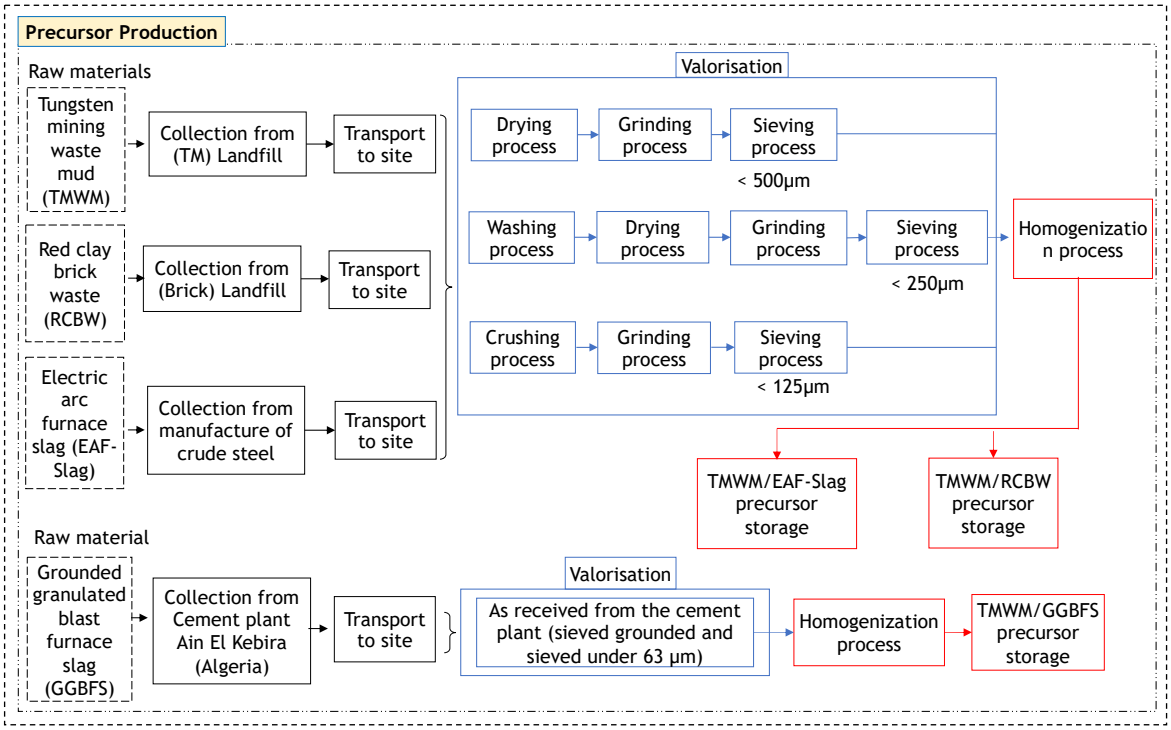

Fig. 2. Processing stages diagram of different wastes used to produce other alkali-activated binders.

3.1.1.1. Tungsten mining waste mud

The main raw material used in this research consisted of tungsten mining waste mud (TMWM); the mining waste was derived as a mix of powder, and coagulation particles form from the Panasqueira tungsten mine in Covilhã, Castelo Branco, Portugal (the "Panasqueira Mine"). The TMWM was dried in the oven at a temperature of 100 °C for 24 h. Afterwards, the dried TMWM was placed into a crush machine and milled to separate the coagulated particles. Finally, the TMWM powder was sieved under 500 µm to be used as the precursor.

In term of chemical composition, TMWM mainly consists of Si (22.3 wt. %), Al (9.8 wt. %), K (3.8 wt. %) and Ca (2.7 wt. %).

3.1.1.2. Red clay brick waste

Red clay brick waste (RCBW) was used as a precursor blended with TMWM in different proportions by volumetric ratios (TMWM/RCBW: 90/10, 80/20, 70/30, 60/40, 50/50 Vt. %). The study is presented in **Paper II**. RCBW is one of the different types of ceramic waste used to develop alkali-activated binders [59]. Many studies and research have been carried out to develop either AAMs or hybrid cement using red clay brick waste as a source of alumina-silicate materials and other minerals. Regarding the RCBW the following processing procedures were adopted: initially, the coarse brick waste was submitted to washing process to remove and separate the contaminations and some other construction impurities (mortar, sand, varnish); the next step was to place it in the oven at a temperature of 60 °C, for 24 h for complete drying; finally, the coarse brick waste was crushed using a crushing device and was sieved to obtain particles of sizes under 250 µm. The chemical composition of RCBW mainly consists of Si (27.9 wt. %), Al (13.3 wt. %) and K (2.44 wt. %).

3.1.1.3. Granulated grounded blast furnace slag

The slag used in **Papers III** and **V** was a ground granulated blast-furnace slag (GGBFS) by-product resulting from the separation of the metal from the ore at the metallurgic unit of El Hadjar located in the north-east of Algeria. The slag is grounded and sieved under 63 µm to be used as a cement additive. The GGBFS has the following chemical compositions: Ca (32.8 wt.%), Si (13.7 wt.%) and Al (3.2 wt.%). The GGBFS has a quality factor $K = (CaO + MgO + Al_2O_3) / (SiO_2 + TiO_2)$ and a coefficient of basicity $Kb = (CaO + MgO) / (SiO_2 + Al_2O_3)$ of 1.79 and 1.35, respectively classifying it as a neutral slag.

3.1.1.4. Electric arc furnace slag

The second type of slag used in **Papers IV** and **VI** was an electric arc furnace slag received in aggregates from the national steel industry in Maia and Aldeia de Paio Pires, Seixal. The EAF-Slag was first dried for 24 hours in the oven at a temperature of 60°C; later, the EAF-Slag aggregates were crushed to transform the EAF-Slag into a powder; finally, the EAF-Slag powder was sieved to get EAF-Slag particle sizes under 125 µm. For EAF-Slag the main oxide compositions are (CaO; 33.3 wt.%), (Fe_2O_3; 30.5 wt.%), (SiO_2; 15 wt.%) and (Al_2O_3; 10.1 wt.%). The basicity coefficient K_b=(CaO+MgO+MnO)/(SiO_2+Al_2O_3) determined for

EAF-Slag was equal to 1.64 [60, 61]. Additionally, the hydraulic modulus (HM) also defined as HM=(CaO+MgO+Al_2O_3)/SiO_2 [62] suggested that the HM of the slag materials should exceed 1.40 to ensure sound hydration property. In the current study, the HM of electric arc furnace slag used is equal to 3.19, reflecting the better hydration properties of electric arc furnace slag.

3.1.1.5. Metakaolin

Metakaolin used in the research was supplied by the chemical company BASF Catalysts LLC. Commercial Metakaolin MetaMAX is a high reactivity metakaolin (HRM) pozzolan produced by thermal activation of high purity kaolin clay within a specific temperature range. MetaMax is a high purity white mineral admixture that meets or exceeds all ASTM C-618 Class N pozzolans specifications and meets the strength activity index as per ASTM C-1240. In **Paper V,** the metakaolin was used as aluminosilicate-rich source material, with 10 wt.% addition, to increase the ternary alkali-activated binder mixture's reactivity. The chemical compositions of MK were calculated in terms of the oxides, which mainly contains SiO_2 (49.75) wt. %), Al_2O_3 (46.54 wt. %), TiO_2 (3.04 wt. %) and Fe_2O_3 (0.67 wt. %).

Table 2 and Table 3, shows the chemical composition of TMWM and other precursors used in this research work.

3.1.2. Physical characterisation of the precursors

The chemical compositions of raw materials were evaluated by Scanning Electron Microscopy with Energy Dispersive Spectroscopy (SEM-EDS) microanalysis, using HITACHI S-3400N microscope equipment. Loss on ignition (LOI) was performed in the temperature range from 25 to 1000°C with a heating rate 10°C min^{-1} in a Helium atmosphere using thermo-gravimetric analysis SDT Q-50 (TA Instrument). The LOI was performed in the temperature range from 25 to 1000°C with a heating rate of 10°C min^{-1} in a Helium atmosphere. Tested powders consisted of about 7 to 10 mg taken from the waste materials and sieved under 75 μm. The particle size distribution of all precursors used in this research is shown in Fig. 3. The particle size distribution of the precursor's powders was determined using laser diffraction (CILAS 1190 apparatus). The precursors' bulk powder densities were determined using a gas displacement pycnometer (model. AccuPyc1340, Micromeritics, Norcross, Georgia apparatus). The Blaine fineness of the different powders was determined according to EN 196-6 (2019) [91], using Blaine air permeability (model. ACMEL LABO BSA1 apparatus).

Table 2. Chemical composition (element), LOI, density, Blaine specific area, and mean particle size of the precursors (TMWM, RCBW and GGBFS).

Component	TMWM (w.%)	RCBW (w.%)	GGBFS (w.%)
O	47.61	48.11	45.34
Si	22.32	27.85	13.68
Al	9.78	13.31	3.24
Ti	0.4	0.62	0.28
S	1.95	0.15	0.34
K	3.76	2.44	0.4
Ca	2.73	0.58	32.81
Fe	7.1	5.61	0.21
Mg	0.79	0.89	2.57
Na	0.93	0.38	0.26
P	-	0.06	-
Zn	0.4	-	-
Cu	0.2	-	0.26
As	1.98	-	-
Mn	0.05	-	0.8
LOI*	11.6	3.88	2.37
Density (g/cm^3)	3.0319	2.7339	2.9266
Blaine specific area (cm^2/g)	1017	3379	2940
Particle size D_{50} (μm)	152.4	40.3	10.91

Table 3. Chemical composition (Oxides), LOI, density, Blaine specific area, and mean particle size of the precursor EAF-Slag and MK.

Component	EAF-Slag (wt. %)	MK (wt.%)
Al_2O_3	10.08	46.54
SiO_2	15	49.75
TiO_2	0.82	3.04
SO_3	0.19	-
K_2O	-	-
CaO	33.29	-
Fe_2O_3	30.48	0.67
MgO	4.54	-
Na_2O	0.13	-
MnO	3.23	-
Cr	2.08	-
ZnO	-	-
LOI*	-	-

Density (g/cm³)	3.703	260
Blaine specific area (cm²/g)	1360	
Particle size D_{50} (μm)	13.01	3.8

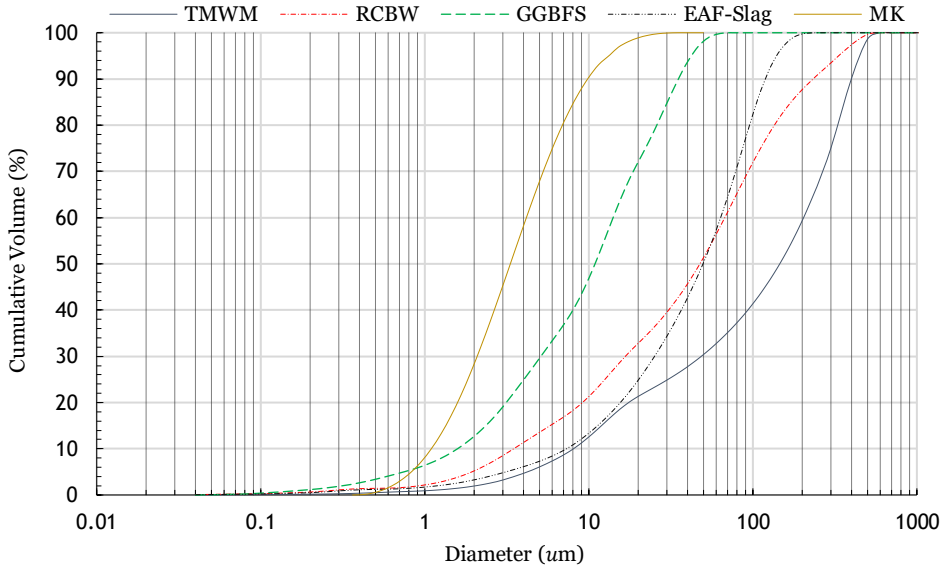

Fig. 3. Particle size distribution of all the precursors used in the research (TMWM, RCBW, GGBFS, EAF-Slag and MK).

3.1.3. Alkaline activator solutions

Sodium silicate (Na_2SiO_3), sodium hydroxide (NaOH), potassium hydroxide (KOH) and dissolved ground glass in sodium hydroxide were used as alkaline activator solutions for the preparation of the binder samples in **Papers II**, **III**, **IV**, **V** and **VI** (Table 4).

Sodium silicate presented the following chemical composition: (8.60 wt.% Na_2O, 27.79 wt.% SiO_2, 63.19 wt.% H_2O, and 0.4 wt.% Al_2O_3). The modulus of a silicate solution is defined as the molar ratio SiO_2/M_2O, where M is an alkali metal. For the sodium silicate solution, the alkali metal is Na then the modulus of sodium silicate solution is SiO_2/Na_2O equal to 3.23. It was supplied by Solvay SA, Póvoa de Santa Iria, Portugal (ref. D40), which cost 0.38 €/Kg. Sodium silicate was used as an alkaline activator in all the study. It was mixed with other activators (SH, Potassium hydroxide and dissolved ground glass in NaOH).

Sodium hydroxide flakes of 98,6% purity were supplied by DOS SANTOS, LDA Portugal, which cost 7.63 €/Kg. Potassium hydroxide flakes of 98% purity were obtained from Quimialmel Chemical Minerals Ltd., Portugal which cost 15.50 €/Kg. The sodium hydroxide and potassium hydroxide solutions were prepared by dissolving NaOH or KOH pellets in

distilled water and cooling 24 hours before use. Sodium hydroxide and potassium hydroxide were dissolved in distilled water to provide the alkaline solutions' required concentration in the alkali-activated mixtures. Sodium hydroxide solution in **Papers II** and **VI** was prepared with the concentration of 10M; however, the concentration of the sodium hydroxide in **Paper V** was 8M. In contrast, the second alkaline activator solution used besides the sodium silicate in **Paper IV** was KOH with the concentration 8M.

The **Paper III** investigation's main objective was to evaluate the effect of the different type of alkaline activator solutions. The activator concentration on the compressive strength and the microstructure of the hybrid alkaline binders, the alkaline activator solutions used in the investigation were divided into three main groups (A, B and C) as follows: the alkaline activators group **A** are a combination of solutions: (66.66 wt.%) Sodium Silicate (SS) (D40) and (33.33 wt.%) 8M Sodium Hydroxide "NaOH". The alkaline activators group B (**B1 and B2)**: are a combination of solutions: (66.66 wt.%) sodium silicate (SS) (D40) and (33.33 wt.%) potassium hydroxide "KOH" for **B1** the molarity of KOH is 8M, and for **B2** the molarity is 10M. The alkaline activators group **C**: are a combination between (66.66 wt.%) Sodium Silicate (D40) and dissolved waste glass powder into sodium hydroxide (33.33 wt.%), i.e. [sodium hydroxide (0.29 wt.%) as a solvent and waste glass powder as solute (0.04 wt.%)] to increase the modulus of alkali silicate solution. The waste glass powder that dissolved in the NaOH solution is a waste glass obtained from ground flint glass bottles using the crushing machine. After, the milled glass powder was sieved, and the particle size was maintained below 45 µm. The chemical composition of glass powder: (12.52% by weight Na_2O, 68.13% by weight SiO_2, and 2.8% by weight Al_2O_3)**.** The dissolution of the glass powder into sodium hydroxide by applying heat and stirring the solution as follows: Sieved the solute (waste glass powder) under 45 µm to obtain a greater surface area, there can be more contact between the particles of the solute (waste glass powder) and the solvent (NaOH 8M). The sodium hydroxide solution and (5 Wt,%) waste glass powder were mixed using Magnetic stirrers "agimatic e selecta" for a period of 48 H at 700 rpm, and a 40 ˚C temperature to increase dissolvability. The waste glass powder was slowly added to the activator solution (sodium hydroxide).

Table 4. The list of alkaline activator solutions used in this research.

Alkaline Solutions	**SS+ SH (10M)**	**SS+ SH (8M)**	**SS+ KOH (8M)**	**SS + SH+ dissolved Glass in SH**
Paper(s)	Papers II, III and VI	Papers III and V	Papers III and IV	Paper III

SS-Sodium silicate
SH-Sodium hydroxide
KOH-Potassium hydroxide

3.2. Methodology

3.2.1. Mixtures design, moulding and curing treatment

Several types of mixtures were studied in the current research to produce binding pastes, based on a combination of TMWM with other mineral wastes, such as RCBW, GGBFS, EAF-Slag and Metakaolin, with different combinations, different types of alkaline activator solutions, and different solid/liquid ratios, as it is shown in Fig. 4. These mixtures were designed to study its influence on the compressive strength results and the microstructure properties of the developed alkali-activated binders.

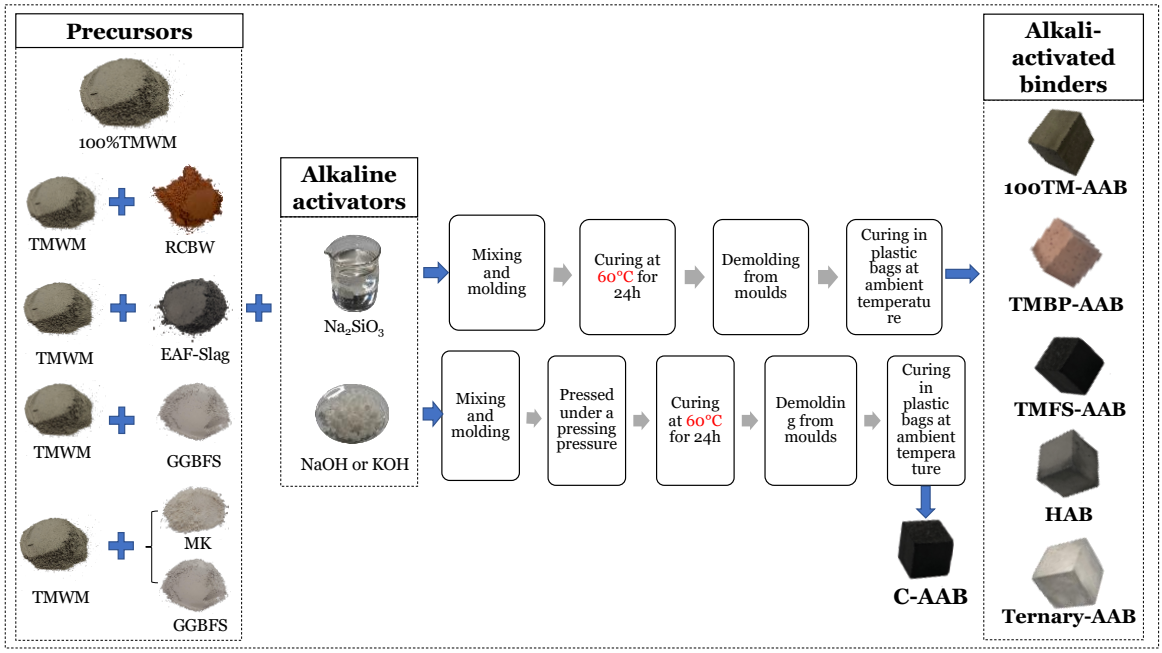

Fig. 4. Mixtures design of the different alkali-activated binders.

3.2.1.1. Alkali-activated binders based on Tungsten mining waste and red clay brick waste

In **Paper II**, the mixtures' precursors were TMWM and RCBW. The ratios between the precursors and the liquid/solid ratio alkaline activator solutions used are presented in Table 5. The initial theoretical Al/Si, Ca/Si, Na/Si and K/Si weight ratios of the alkali-activated

admixtures are shown in Table 6. The initial theoretical ratios are changed with the change of the RCBW content in the mixtures.

Table 5. Formulation of the alkali-activated binders based on Tungsten mining waste (TMWM) and red clay brick waste (RCBW) activated by Sodium silicate (SS) and sodium hydroxide (SH).

Paper II	Precursors		Alkaline Solutions		Solid/liquid mass ratios
	TMWM (Vt. %)	RCBW (Vt. %)	SS (D40)	SH (10M)	
RCBW01TMWM09	90	10	2	1	3
RCBW02TMWM08	80	20	2	1	3
RCBW03TMWM07	70	30	2	1	3
RCBW04TMWM06	60	40	2	1	3
RCBW05TMWM05	50	50	2	1	3

Table 6. The initial theoretical Al/Si, Ca/Si, Na/Si and K/Si weight ratios of the alkali-activated binders based on Tungsten mining waste (TMWM) and red clay brick waste (RCBW).

Paper II	Ratios			
	Al/Si	Ca/Si	Na/Si	K/Si
RCBW01TMWM09	0.462	0.018	0.191	0.098
RCBW02TMWM08	0.51	0.019	0.204	0.104
RCBW03TMWM07	0.568	0.021	0.22	0.11
RCBW04TMWM06	0.641	0.023	0.24	0.117
RCBW05TMWM05	0.734	0.025	0.266	0.127

3.2.1.2. Hybrid alkaline binder based on tungsten mining waste and granulated grounded blast furnace slag

Paper III focus was to investigate the effect of the different type of the alkaline activators, the molarity of the activators, and the solid to liquid ratios on the compressive strength development and the microstructure properties of the hybrid alkaline binders. The Precursors used in **Paper III** were TMWM/GGBFS in a fixed ratio (90/10 Vt. %) using different alkaline activator solutions, various combinations of activators and different S/L ratios, as it is shown in Table 7. The initial theoretical Al/Si, Ca/Si, Na/Si and K/Si weight ratios of the different hybrid alkaline binder mixtures are given in Table 8.

Table 7. Formulation of the alkali-activated binders based on Tungsten mining waste (TMWM) and grounded granulated blast furnace slag activated by Sodium silicate (SS), sodium hydroxide (SH), potassium hydroxide (KOH) and dissolved glass in SH with Solid/liquid mass ratios.

Paper III	Precursors		Ratio of activators combination (wt.%)					Solid/liquid mass ratios
	TMWM (Vt. %)	GGBFS (Vt. %)	SS	SH 8M	KOH 8M	KOH 10M	Waste glass powder	

HAB1	90	10	0.67	0.33	-	-	-	3
HAB2	90	10	0.67	0.33	-	-	-	4
HAB3	90	10	0.67	-	0.33	-	-	3
HAB4	90	10	0.67	-	0.33	-	-	4
HAB5	90	10	0.67	-	-	0.33	-	4
HAB6	90	10	0.67	0.29	-	-	0.04	3

Table 8. The initial theoretical Al/Si, Ca/Si, Na/Si and K/Si weight ratios of the hybrid alkaline binders activated by different alkaline activator solutions.

Paper III	**Ratios**			
	Al/Si	**Ca/Si**	**Na/Si**	**K/Si**
HAB1	0.482	0.119	0.211	0.104
HAB2	0.454	0.112	0.214	0.098
HAB3	0.452	0.112	0.118	0.077
HAB4	0.465	0.115	0.104	0.059
HAB5	0.452	0.112	0.118	0.068
HAB6	0.452	0.112	0.198	0.098

3.2.1.3. Alkali-activated binders based on Tungsten mining waste and electric arc furnace slag

The formulation of the mixtures prepared in **Paper IV** is presented in Table 9. The alkali-activated mixtures were prepared using TMWM and EAF-Slag as precursors. The blended EAF-Slag with TMWM in different proportion was to investigate the effect of different dosages of EAF-Slag on the compressive strength development and microstructure properties of the tungsten mining waste-based alkali-activated binder. The EAF-Slag was added to the TMWM mixtures in increasing proportions (10, 20, 30, 40 and 50 Vt. %). The powders mixtures (TMWM and EAF-Slag) were mixed with the alkaline activator solutions with S/L ratio 3. The initial theoretical Al/Si, Ca/Si, Na/Si and K/Si weight ratios of the tungsten mining waste and electric arc furnace slag are given in Table 10.

Table 9. Formulation of the alkali-activated binders based on Tungsten mining waste (TMWM) and electric arc furnace slag (EAF-Slag) activated by sodium silicate (SS) and potassium hydroxide (KOH).

Paper IV	**Precursors**		**Alkaline Solutions**		**Solid/liquid mass ratios**
	TMWM (Vt. %)	**EAF-Slag (Vt. %)**	**SS (D40)**	**KOH (8M)**	
100TMWM	100	0	2	1	3
10EAF-Slag90TMWM	90	10	2	1	3
20EAF-Slag80TMWM	80	20	2	1	3
30EAF-Slag70TMWM	70	30	2	1	3
40EAF-Slag60TMWM	60	40	2	1	3

50EAF-Slag50TMWM	50	50	2	1	3
100EAF-Slag	0	100	2	1	3

Table 10. The initial theoretical Al/Si, Ca/Si, Na/Si and, K/Si weight ratios of the TMWM and EAF-Slag-based alkali-activated binders

Paper IV	**Ratios**			
	Al/Si	**Ca/Si**	**Na/Si**	**K/Si**
100TMWM	0.457	0.018	0.128	0.044
10EAF-Slag90TMWM	0.437	0.125	0.127	0.045
20EAF-Slag80TMWM	0.416	0.235	0.125	0.046
30EAF-Slag70TMWM	0.395	0.349	0.123	0.048
40EAF-Slag60TMWM	0.372	0.465	0.121	0.049
50EAF-Slag50TMWM	0.349	0.586	0.118	0.05
100EAF-Slag	0.223	1.25	0.107	0.058

3.2.1.4. Ternary alkali-activated binder based on tungsten mining waste, granulated grounded blast furnace slag and metakaolin

Three types of materials were used to formulate the Ternary-AAB (80 wt.% TMWM + 10 wt.% GGBFS + 10 wt.% MK) in **Paper V**. The ternary precursors were mixed in a container and agitated to ensure the homogeneity of the precursor. After that, the precursors were activated with the alkaline activator solution (2/3 sodium silicate + 1/3 NaOH 8M), using a solid/liquid ratio of 2.5. The formulation of the alkali-activated binders based on tungsten mining waste (and the ternary alkali-activated binder are given in Table 11. The initial theoretical Si/Al, Ca/Si, K/Al and Na/Si weight ratios of the tungsten mining waste-based alkali-activated binder and the ternary alkali-activated binder are given in Table 12.

Table 11. Formulation of the alkali-activated binder based on Tungsten mining waste (TMWM-AAB) and ternary alkali-activated binder (Ternary-AAB).

Paper V	**Precursors**			**Alkaline Solutions**		**Solid/liquid mass ratios**
	TMWM (wt. %)	**GGBFS (wt. %)**	**MK (wt. %)**	**SS (D40)**	**SH (10M)**	
TMWM-AAB	100	0	0	2/3	1/3	2.5
Ternary-AAB	80	10	10	2/3	1/3	2.5

Table 12. The initial theoretical Si/Al, Ca/Si, Na/Si and K/Al weight ratios of the alkali-activated binders based on Tungsten mining waste (TMWM-AAB) and the ternary alkali-activated binder (Ternary-AAB).

Paper V	**Ratios**			
	Si/Al	**Ca/Si**	**K/Al**	**Na/Si**
TMWM-AAB	2.719	0.014	0.311	0.171

Ternary-AAB	2.122	0.123	0.239	0.391

3.2.1.5. Low liquid to solid binary alkali-activated binder

For the low liquid-to-solid alkali-activated binder studied in **Paper VI**, the alkali-activated binder samples' preparation was as follows: 50 Vt. % of TMWM powder blended with another 50 Vt. % of EAF-Slag. The low liquid-to-solid binary TMWM-EAF-Slag alkali-activated material mixtures were made by mixing the raw powders with an alkaline activator solution (12.5% alkaline activator solution calculated from the total weight of the precursors). The liquid to solid ratio (L/S) was about 11.11% of the mixture's total weight (Table 13). The initial theoretical Al/Si, Ca/Si, Na/Si and, K/Si weight ratios of the low liquid to solid alkali-activated binder are shown in Table 14.

Table 13. Formulation of the low L/S ratio alkali-activated binder based on tungsten mining waste and electric arc furnace slag activated by Sodium silicate (SS) and sodium hydroxide (SH) using low L/S ratio.

Paper VI	**Precursors**		**Alkaline Solutions**		**L/S mass ratio**
	TMWM (Vt. %)	**EAF-Slag (Vt. %)**	**SS (D40)**	**SH (10M)**	
Mix	50	50	2/3	1/3	0.125

Table 14. The initial theoretical Al/Si, Ca/Si, Na/Si and, K/Si weight ratios of the low L/S ratio alkaline activated binder.

Paper VI	**Ratios**			
	Al/Si	**Ca/Si**	**Na/Si**	**K/Si**
Pressed AABs	0.566	0.957	0.162	0.101

The following steps prepared the alkali-activated formulations studied in **Papers II, III, IV**, and **V**: All the alkali-activated mixes were prepared at room temperature. First, the precursors were dry mixed together in a container and agitated to get a homogeneous powder. Then, the alkaline activator solution was blended with the precursors' powder with different L/S ratios. The resulting mixtures of the precursor and the alkaline activator solution were mechanically stirred together using a Hobart mixer with a mixing time of five minutes (about 3 minutes at low speed followed by 2 minutes at high speed). The alkali-activated pastes were poured into the curing moulds (with the dimensions 150 × 25 × 25 mm) by gravity. Afterwards, the moulds were hand vibrated for 2 minutes. After mixing and moulding, the filled moulds were stored in an oven at a temperature of 60 °C for 24 h. For synthesis and to avoid water evaporation of the AABs during curing, the filled moulds were wrapped with plastic film during the oven curing synthesis. After the initial 24 hours

oven curing period, the specimens were de-moulded and were left to cure in laboratory condition (open-air and about 20 °C) and were placed inside sealed plastic bags, until being tested after (1, 3, 7, 14, 28, 56 and 90 days). The hardened binder samples were cut to have a cubic dimension (25 cubic mm) using a masonry block saw with a small disc diameter to avoid micro-cracks.

For the low liquid-to-solid alkali-activated binder studied in **Paper VI**, the alkali-activated binder samples' preparation was as follows: the blended powders were hand-blended for 60 seconds to get homogeneous powder. The mixture powder blended with the alkaline activator solution for about 180 seconds to obtain a low liquid-to-solid binary TMWM-EAF-Slag alkali-activated mixture. The obtained mixture was cast into 20 mm× 20 mm× 20 mm lubricated cubic-shaped steel moulds, vibrated for compaction, and pressed under a pressing pressure ranging 20, 40, 60, 80, 100 MPa, and then sealed with a plastic sheet as to minimise loss of evaporable water. Afterwards, the samples were left to cure undisturbed at 60 ◦C for 24 h, and then air-cured at room temperature up to 7, 14 and 28 days and then exposed to compressive strength measurements.

In the current research the different initial theoretical aluminium/silicon (Al/Si), calcium/silicon (Ca/Si), sodium/silicon (Na/Si) and potassium/silicon (K/Si) atomic weight ratios, are investigated in all the papers. These atomic weight ratios were calculated by including the mixtures' chemical composition containing both precursors and activator solutions. This approach implicitly assumed the total dissolution of the starting precursors. The ratios include the chemical composition of the precursors and the chemical composition of the alkaline activator solutions. But in fact, the precursors were not fully dissolved (existence of unreacted particles) which is observed in the (SEM-EDX) images in **Papers II, III, IV** and **V.** The variation of initial theoretical ratios affects the compressive strength and the microstructure properties of all types of binders developed in this research.

3.3. Analytical techniques

3.3.1. Compressive strength development

The specimens' compressive strength was determined using a 3000 kN electro-hydraulic mechanical testing machine "ADR Touch 3000 BS EN Compression Machine with Digital Readout and Self Centring Platens", with a loading rate of 0.05 kN/Second.

The compressive strength tests were performed on 25 cubic mm-sized samples in **Papers II, III, IV** and **V**. However, in **Paper VI,** the compressive strength data were collected using 20 mm cubic-sized specimens. For each period and paste type, five specimens were tested, and the results were averaged. The samples were tested after 1, 3, 7, 14 and 28 days of curing in **Paper II**. In the hybrid alkaline binders, the samples were tested after 7, 14, 28 and 90 days of curing in **Paper III**. For the **Papers IV** and **VI** the samples were tested after 7, 14 and 28 days of curing.

3.3.2. TG-DTG analyses

Thermogravimetric (TG) and Differential Thermogravimetric (DTG) analyses were carried out on an SDT Q-50 (TA Instrument). In **Papers II** and **III**, all the TG-DTG experiments were performed in the temperature range from 25 to 1000°C with a heating rate of 10°C min^{-1} in a Helium atmosphere. Tested specimens consisted of about 7 to 10 mg of the powdered specimen collected from the remains of the crushed specimens on which the compressive strength tests were applied. After milling, the powder to be tested was sieved under 75 µm. For testing purposes, the specimens were placed in a platinum crucible and heated from ambient temperature to 1000°C.

3.3.3. X-ray diffraction analyses

The crystalline phases of the powdered precursors (TMWM, RCBW, GGBFS and EAF-Slag) and the resulted AABs specimens were identified by XRD using a Rigaku model D-Max III/C equipment, with Cu tube and K-α radiation (40 kV, 40 mA). The 2θ operational range was from 5° to 90°. In **Paper II** the calculation of crystallinity of the precursors (TMWM and RCBW) by XRD was based on the presumption that the broad peak comes from amorphous phases; the sharp peak comes from crystal phases. The software (MDI jade 6.5) calculates the degree of crystallinity using the equation (1):

$$Crystallinity\ (\%) = \frac{Total\ area\ of\ crystalline\ peaks * 100)}{Total\ area\ of\ all\ peaks} \quad \text{.....(1)}$$

The X-Ray Diffraction (XRD) analysis was chosen to analyse the raw materials, and the alkali-activated binders in **Papers II, III** and **IV**. The alkali-activated powders were selected from the crushed AABs samples (AABs were smashed using marble rod). Both powders (raw materials and AABs) were sieved under 75 μm before testing. The XRD sample preparation was as follows: first, the samples were extremely finely grained to achieve adequate signal to noise ratio (and avoid fluctuation in intensity). After, the powder (ground sample) was spread in the sample holder. Then, a microscope glass was used to press in the powder. After that, a Stanley knife or glass plat was used to remove the surplus of powder. Finally, the samples showed a smooth and flat sample surface. The qualitative analysis was assessed using the "MDI jade 6.5" software and the Powder Diffraction File (PDF-2) database.

3.3.4. Microstructural analysis

The Scanning Electron Microscopy (SEM) for the chemical analysis of the raw materials and all the binders was carried out using a Hitachi S-4800 microscope instrument at an accelerating voltage of 15 kV. In **Paper II,** SEM analysis was performed in a backscattered mode (BSE). The 28 days alkali-activated samples were epoxy impregnated and polished before testing, for the characterisation and analysis of the surface morphology and microstructure the binders made in **Paper II**. The EDS (Energy Dispersive X-ray) analyses were carried out using a Bruker Xflash 5010 Cooled by Peltier with a resolution of ≤ 129 eV of the Mn Detector EDS instrument. **Papers II** and **III** presented the SEM-EDS analysis of tungsten mining waste mud, red clay brick waste and grounded granulated blast furnace slag powders. In the current research, the specimens examined by (SEM-EDS) were selected from cleaned small fractured pieces of the binders taken from the original 28 days samples to use under the back-scattered electron detector (BSE). The Tested binders' specimens were coated with gold before the SEM-EDS examination to improve the samples' imaging at the SEM. The microstructural analyses were performed to see and compare the reaction products, and the matrix structures of the different binders paste in **Papers II, III, IV,** and **V**.

3.3.5. Fourier Transform Infra-Red analyses

Fourier transform infrared (FT-IR) spectroscopy data were obtained to examine the precursors used in this research and the local structure of the reaction products in each alkali-activated binder samples of **Papers II, III, IV, V,** and **VI**. The FT-IR analyses

spectra were recorded from 600 to 4000 cm^{-1} using Nicolet iS10 FT-IR Spectrometer (Thermo Scientific), Smart iTR accessory instrument by diamond HATR crystal.

3.3.6. Mercury Intrusion Porosimetry analyses

Mercury intrusion porosimetry (MIP) analysis method was used to investigate the binders' pore structure resulting in **Papers II, III** and **IV**. This research MIP analysis was performed using Micromeritics AutoPore IV 9500 V1.07 with maximum and minimum applied pressures of 413.7 MPa and 3.63 kPa, corresponding to a minimum pore size of 5 nm and maximum pore size of 345 μm. For MIP testing, a specimen with a weight of (1.5-2.5 g) was taken from the original sample using metal chisel after 28 days of cure. The samples were left in a glass desiccator containing silica gel to ensure the removal of the samples' moisture.

4.Results and discussion

4.1. Characterisation of the raw materials

4.1.1. Mineralogical analyses

The XRD analysis of the powdered precursors (TMWM, RCBW, GGBFS, EAF-Slag) studied in this investigation were shown in **Papers II, III** and **IV**.

To determine the influence the degree of crystallinity has on the activation of the precursor, a series of XRD tests were conducted on raw materials (TMWM, RCBW). The XRD analyses show that both powders (TMWM and RCBW) had almost the same crystallinity degree (85% and 89%). The XRD patterns of TMWM shown in Fig. 5-a indicate their crystalline nature and consist mainly of Muscovite and Quartz (SiO_2), which were identified by their characteristic, as follows: muscovite (Ref. PDF#46–1409), quartz (Ref. PDF#46–1045) and clinochlore (ref. PDF#29–0701). Muscovite is a dioctahedral layered structure in which a sheet of octahedral Al ions is sandwiched between two sheets of linked SiO_4 tetrahedral with a general formula $KAl_2(Si_3Al)O_{10}(OH)_2$.

The X-ray diffractogram spectra of RCBW, as presented in Fig. 5-b indicates the semi-crystalline degree of the waste material and the presence of Quartz SiO_2 (Ref. PDF#46–1045) as the main phase. Besides the quartz, there are other main crystalline phases in the RCBW: Illite, Muscovite, Hematite and Mullite. The absence of other crystalline phases in RCBW is possibly due to the low firing temperature of the recycled brick used in the investigation. According to Ahmad et al.[63], the absence of some crystalline phases in the samples investigated in their studies was also because of the low firing (under 1000 °C) of the bricks tested.

To increase the reactivity of the admixtures studied in **Papers III** and **IV**, GGBFS was blended with TMWM as precursors. The GGBFS is predominantly amorphous. Indicated by a wide and diffusive reflection in the interval of 05-90° angles 2θ (Fig. 5-c), consist of Quartz (Ref. PDF#46-1045), Gehlenite ($Ca_2Al[AlSiO_7]$) (Ref. PDF#87-0968), Akermanite ($Ca_2Mg[Si_2O_7]$) (Ref. PDF#35-0592), Calcite ($CaCO_3$) (Ref. PDF#47-1743) and depolymerised calcium silicate glasses. Meanwhile, the dispersion peaks between 15° and 50° are the characteristic peaks for the glass phases of GGBFS. For the X-ray diffraction (XRD) analysis of the EAF-Slag used as a precursor in **Papers IV** and **VI**, the EAF-Slag present very complex XRD spectra as shown in Fig. 5-d. Different mineral phases with

distinct peaks of high intensities and some overlapping peaks of low intensities were detected. The slow cooling conditions of the EAF-Slag allows the formation of various crystalline phases [64]. The primary ones being: Magnetite (Ref. PDF#08-0479), Calcite (Ref. PDF#86-2339), Siderite (Ref. PDF#83-1764), Gehlenite (Ref. PDF#87-0968), Wustie (Ref. PDF#06-0615) and Calcium Silicate (Ref. PDF#20-0237).

-a) TMWM

Q: Quartz
M: Muscovite
C: Clinochlore

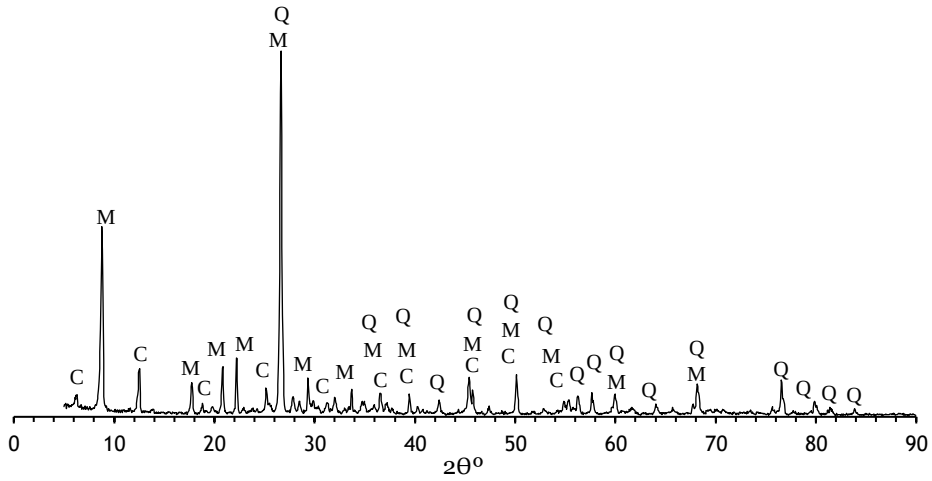

-b) RCBW

Q: Quartz ; M: Muscovite
I: Illite ; H: Hematite
R: Rutile ; Mu: Multite

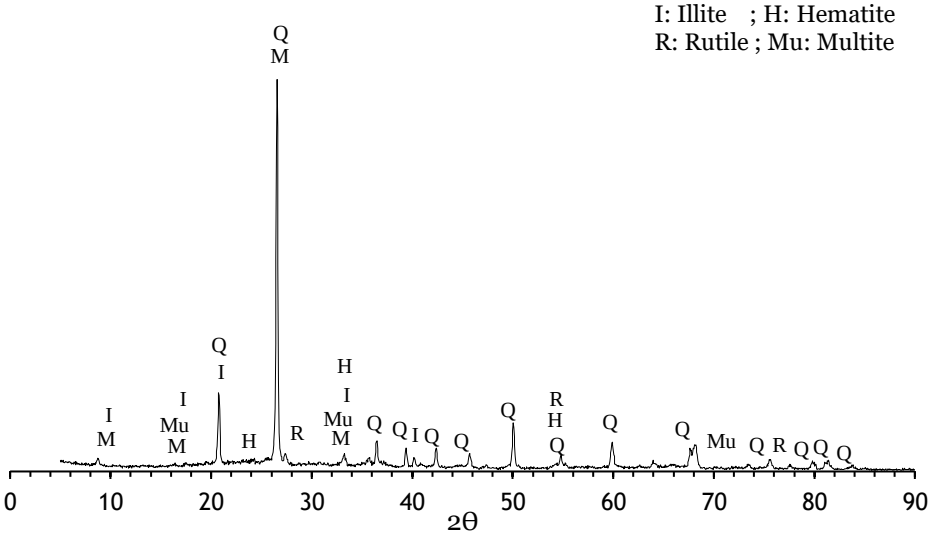

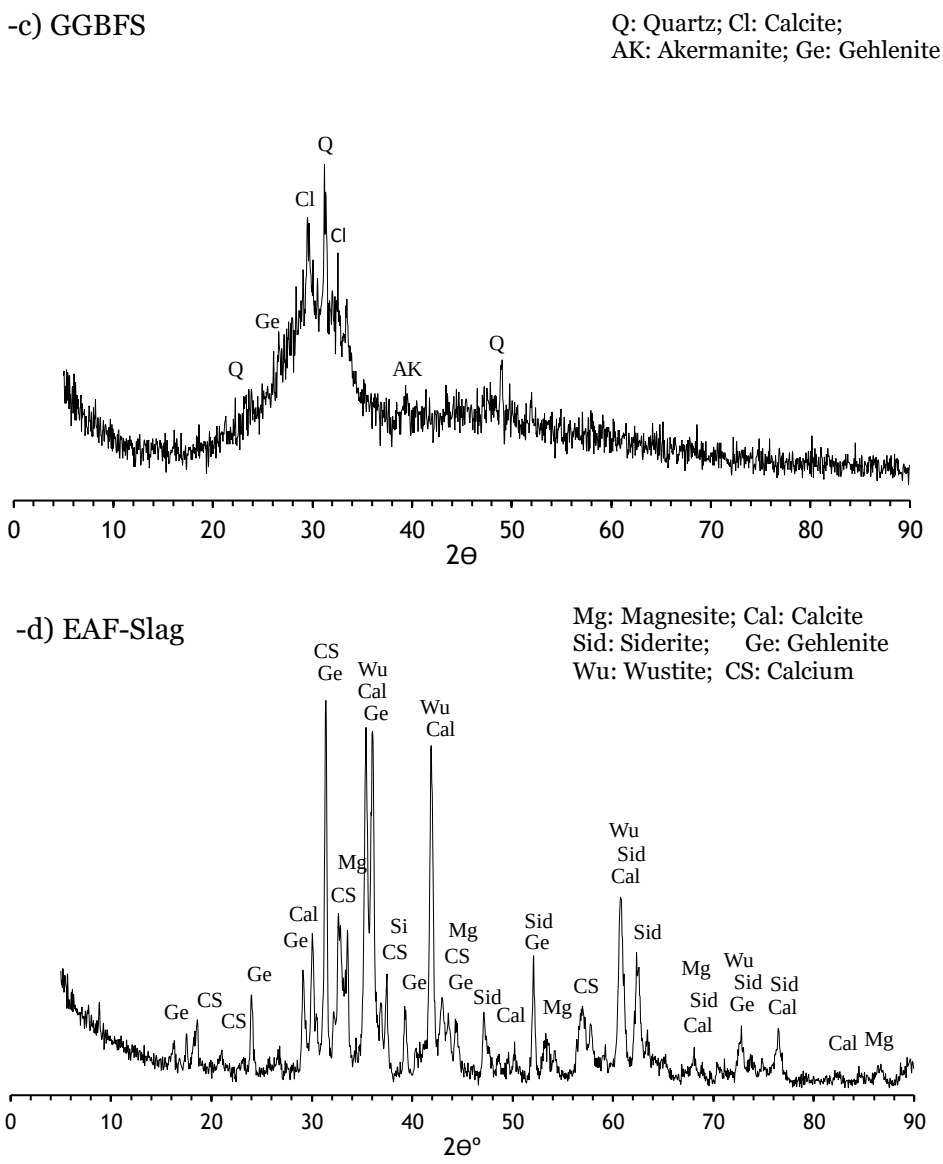

Fig. 5. X-ray diffractograms of: a)-TMWM; b)- RCBW, c)- GGBFS, and d)-EAF-Slag.

4.1.2. TG-DTG analyses

Thermogravimetric and Differential thermogravimetric results show different trends in the precursors' weight loss (TMWM, RCBW and GGBFS) as reported in Fig. 6. The increase of the heating temperature-induced slight reductions in the weight of the precursor powders. The TG-DTG analysis of TMWM, RCBW and GGBFS powders were demonstrated in **Papers II** and **III**. The TMWM sample lost 7.31% from its total weight during the heating analysis. The curves show different weight loss stages, which start with the first temperatures ranging from 30°C up to 400°C only minor mass changes loss were identified in TMWM sample about 0.24%. This mass loss can be attributed to water loss via evaporation. The most significant mass changes observed took place between 450 °C and 1000 °C. A significantly mass reduction was 2.96% at the temperature range between 475°C

and 650 °C, the DTG peak at the temperature of 499 °C due to the dehydroxylation and de-ammoniation [loss of NH_4 or decomposition of NH_4 of muscovite content in the raw TMWM; the dehydroxylated phase has larger unit-cell parameters and the coordination of Al atoms changes from 6 to 5]. The dehydroxylation process is expected to be described by the reaction $2(OH) \rightarrow H_2O+O$ (residual oxygen); moreover, the dehydroxylation of muscovite is complex and affected by heating rates, temperature, pressure, grain size, chemical composition, defects, and other factors [65]. The mass loss observed in Fig. 6a between 400 °C and 650 °C also belongs to partial clinochlore decomposition by interlayer dehydroxylation [66]. The sample shows a loss of 0.94% between the temperatures range (900 °C-985 °C) which is possibly related to the effect of K_2O and Na_2O constituents fluxes when the TMWM started to react around 900 °C [67]. While the TG-DTG of the precursor (RCBW) was studied in **Paper II**, the RCBW powder loss 3.88% of its total weight. The first 0.50% decrease in the mass occurred between 490 and 525 °C and between 570 to 612 °C range which may be due to the removal of chemical water. The highest weight loss (2,80%) was detected between 677 to 900 °C, which is possibly related with the dihydroxylation of 'illite' content in the RCBW sample [68, 69]. It is also due to the loss of the combined water in clay minerals, which causes the breakdown of the crystalline clay network [70]. The loss of 0.58% between 900 to 985 °C is possibly related to the effect of K_2O and Na_2O constituents fluxes, such as in TMWM [69, 71].

The TG-DTG curve of GGBFS powder in **Paper III** shows that the GGBFS powder sample lost 3.37% from its total weight. However, the first mass reduction was 0.66% from the ambient temperature up to 500 °C, which is related to removing the sample's moisture and evaporable water content. Also, the only intense peak shown in the DTG curve was at the temperature of 595 °C located at temperatures range of 300°C -750°C corresponding to the decomposition of carbonate species of 300°C-750°C which might correspond to the decomposition of calcite [72, 73]. Moreover, the TGA curve shows a complex pattern of mass changes with slight increase outcome from the mass gain caused by oxidation of sulfides phenomena at the temperatures range (888°C to 1000°C) where the formation of gases (H_2S and SO_3) and solids (e.g. $CaSO_4$) from sulfides present in the raw GGBFS [74].

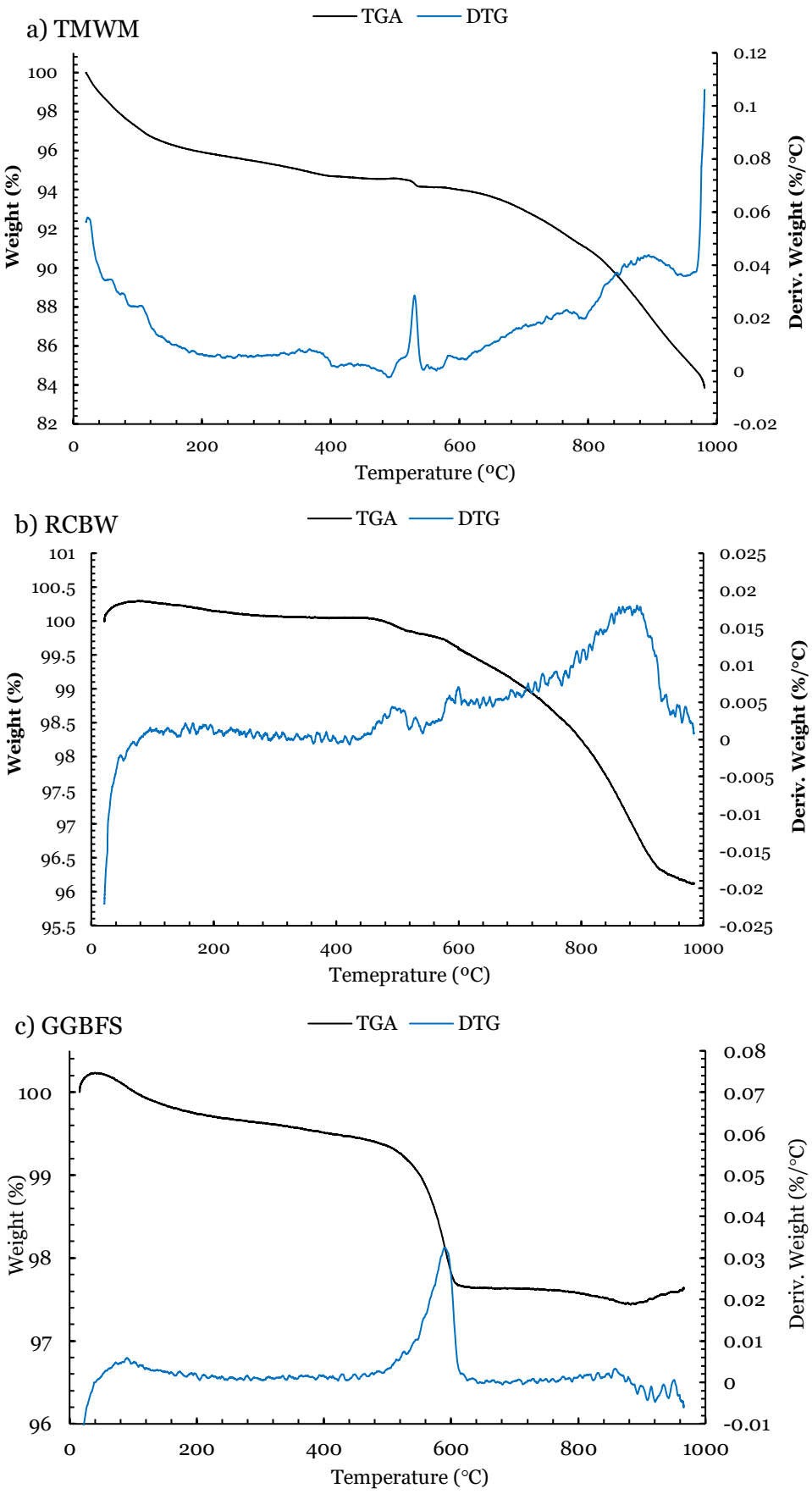

Fig. 6. TG-DTG curves for: a) TMWM, b) RCBW and c) GGBFS.

4.2. Characterisation of the developed binders

4.2.1. Compressive strength development of the binders

Tungsten mining waste mud in its natural state (without calcination) is a low reactive material under the influence of an alkaline medium condition and need to blend with reactive materials (alumina-silicate rich source materials) to produce an hardened matrix. The compressive strength of the samples prepared with 100% TMWM were studied in **Papers IV** and **V**. The blended of TMWM with other mineral waste samples were studied in **Papers II, III, IV** and **V.** The focus in **Paper VI** was to study the effect of the different compressing pressure on the compressive strengths of the low liquid to solid alkali-activated binders.

4.2.1.1. Compressive strength of tungsten mining waste based-alkali-activated binders

The compressive strength of the alkali-activated binders results shows that the samples prepared with 100% TMWM exhibit a very low compressive strength results compared to those prepared with blended precursors at any tested ages.

The alkaline activation of 100% TMWM powder in this research was investigated using two different alkaline activator solutions (SS and KOH 8M and SS+ NaOH 8M). In both tungsten mining waste-based alkali-activated binders the results of the compressive strength reach a low value. For the 100-TMWM-AAB samples activated by SS and KOH 8M in **Paper IV**, the AAB samples' compressive strength at 28 days reached 11.2 MPa. However, in **Paper V** the mixture 100% TMWM activated with SS and NaOH 8M the compressive strength of the AAB samples at 28 days reached 10.7 MPa (Fig. 7).

4.2.1.2. Compressive strength of blended TMWM with other mineral wastes-based alkali-activated binders

This research aimed to enhance the compressive strength results of the tungsten mining waste-based alkali-activated binder. Therefore, the tungsten mining waste mud powder was blended with different types of alumina-silicate rich materials such as red clay brick waste, granulated grounded blast furnace slag, electric arc furnace slag and metakaolin. It was noted that there was an enhancement in the compressive strength results when the TMWM powder was blended with the alumina-silicate rich material powders in different proportion. In **Paper II** and **IV,** greater compressive strength results were obtained when

the second waste materials (RCBW and EAF-Slag) content increased in the precursor admixtures.

For the study in **Paper II,** when the TMWM powder was blended with RCBW powder, the compressive strength of the binders increased with the increase of RCBW powder content in the mixtures. The sample containing the highest proportion of RCBW (50 Vt. %) exhibits the highest compressive strength at 28 days with 58 MPa. In **Paper IV** the TMWM was blended with EAF-Slag in different proportions to improve the AAB samples' compressive strength. The compressive strength of the sample prepared with 50 Vt. % EAF-Slag was obtained at 28 curing days.

For the ternary mixture (80 wt.% TMWM powder was blended with 10 wt. % of GGBFS and 10 wt. %) studied in **Paper V**, the development of the compressive strength of the binder are shown in Fig. 7. The compressive strength results of the ternary alkali-activated binder demonstrate a highest compressive strength value of 50.8 MPa at 28 days curing age, compared to the compressive strength of the samples prepared with 100% TMWM which reach compressive strength value of 10.7 MPa at 28 days curing age.

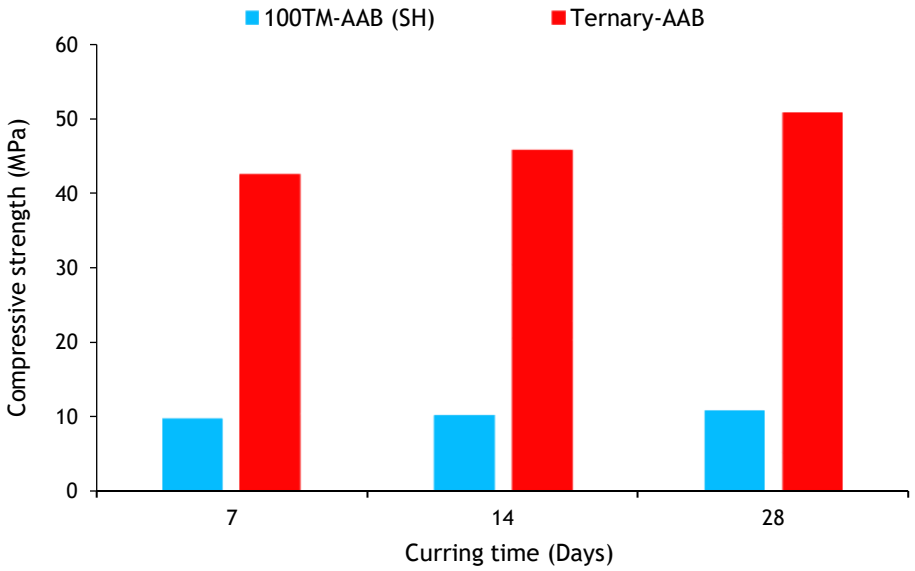

Fig. 7. Compressive strength development of Tungsten mining waste-based alkali-activated binder and the ternary-alkali-activated binders over time.

Paper III focused on the effect of the alkaline activator solutions, the activators' molarity, and the S/L ratio on the binders' compressive strength results development. In the study, the precursors were fixed as 90 Vt. % TMWM blended with 10 Vt. % of GGBFS to increase the mixtures' reactivity. The samples made with solid/liquid ratio= 4, and alkaline activator SS+NaOH 8M gained the highest compressive strength (25 MPa) in early ages (before 28

days), but surpassed by those samples made with the alkaline activator solutions (SS+KOH 8M or 10M and SS+ NaOH 8M+ dissolved Glass in NaOH 8M) with compressive strengths of 29.6 MPa and 33.05 MPa, at 90 days. It was noticed that the compressive strength does not variate so much in the samples made with the same type of activator (sodium silicate and potassium hydroxide) and the same solid/ liquid ratio (4) and different molarity (8 M and 10 M).

To reduce the alkaline activator solutions in the AAB admixtures (low liquid to solid ratio), the AAB samples were prepared with 50 vt. % of TMWM blended with 50 Vt. % EAF-Slag and exposed to different compressing pression (**Paper VI**). The compressive strength results of the low liquid to solid alkali-activated binder shown a good result in producing these types of materials. The compressive strength increases with the increase of the compressing pressure applied to the samples. A greater compressive strength result of 50.6 MPa was obtained after 28 curing days, for the samples subjected to a compressing pressure of 100 MPa. The compressive strengths of all the developed binders in this research are presented in Fig. 8.

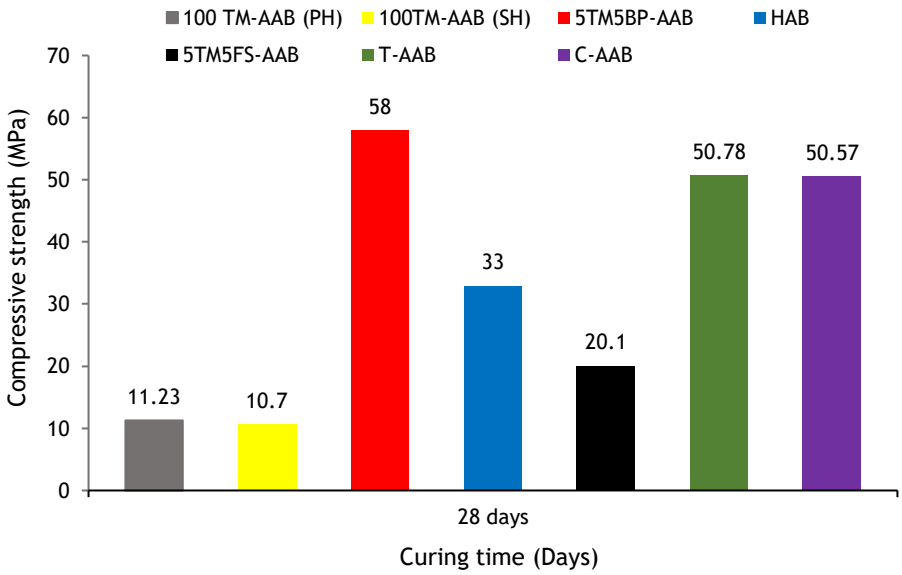

Fig. 8. Compressive strengths development of Tungsten mining waste-based alkali-activated binder and all the blended alkali-activated binders' systems at curing time of 28 days.

4.2.2. Thermogravimetric and differential thermal analyses

The simultaneous thermogravimetric and differential thermal analyses of the TMWM-RCBW alkali-activated and the hybrid alkaline binder specimens were studied in **Papers II** and **III**.

The specimens' TG-DTG analyses show a general idea about the unreacted compositions and the hydration products formed in the matrix after the precursors' alkaline activation. The TG-DTG analysis represent different rates of mass losses in the AAB specimens. The effect of the different dosages of RCBW in the mixtures was investigated in **Paper II**. The TG-DTG analyses represent different rates of mass losses in the binder specimens. The effect of the different types and molarity of alkaline activators and the L/S ratios were studied in **Paper III**. In the TG-DTG analyses of the developed binders in **Papers II** and **III**, it was difficult to estimate the quantities of the reaction product phases formed in the different blended tungsten mining waste mud and other mineral wastes-based alkali-activated binder samples. The estimation formed reaction product phases was based on the weight losses, because the dehydration and decomposition of the alkaline activation gel products are in the same loss of temperature range of the adsorbed free water or evaporable water present on the surface and porosity, and also might due to the chemical bond water.

4.2.3. Microstructure analysis of the binders

The microstructure study was undertaken to observe the matrix structure of the different binder specimens, including the effect of varying mix formulation on the microstructure in **Papers II, IV** and **V**. The impact of the types and the molarity of the activators and the L/S ratios on the microstructure are presented in **Paper III**. Scanning Electron Microscopy (SEM) was used to record micrographs while energy dispersive X-ray spectroscopy (EDS) was an additional tool for the semi-quantitative analysis. The results obtained from EDS analysis in this research were the atomic percentage of each element. Only the major elements are shown together with the calculated Ca/Si, Al/Si and Al/Ca ratios.

4.2.3.1. Microstructure analysis of tungsten mining waste-based alkali-activated binder

The microstructure of the tungsten mining waste-based alkali-activated binder (sample prepared with 100 %TMWM and SS+KOH 8M as activator solutions) is presented in **Paper IV**. The SEM image in Fig. 9 shows the three main features in all the alkali-activated samples: (1) Unreacted particles, (2) Reaction products and (3) Micro-cracks. The 100TM-AAB had relatively poor surface conditions with a high quantity of unreacted particles (irregular shape geometry) embedded in the matrix and partially covered by reaction products and small needle-like phase dispersed on the matrix's surface. The presence of the needles in the 100TM-AAB sample after the alkaline activation may correspond to the formation of carbonates (such as potassium carbonate (K_2CO_3) and sodium carbonate

(Na_2CO_3)). The existence of a high quantity of unreacted particles was due to the low reactivity of TMWM precursor (its natural crystalline mineralogy). After the alkaline activation kinetics of TMWM, SEM-EDS analyses confirmed the formation of two types of reaction product phases, i.e., sodium alumina-silicate hydrates (N-A-S-H) and (sodium, calcium)-alumina-silicate hydrates (N, C)-A-S-H. The formation of (N-A-S-H) due to the high content of the elements (Si, Al, Na) in the mixture.

Moreover, the formation of hybrid reaction product phases (sodium, calcium)- alumino-silicate hydrates (N, C)-A-S-H, corresponded to a different gel obtained for the mixtures with low Ca content in the precursor. The presence of the needles in the 100TM-AAB after the alkaline activation may correspond to the formation of Natrite (Na_2CO_3) needles due to the low reactivity of TMWM, while part of Na content in the mixture remained unreactive. During the curing time, the Na reacted with the CO_2 in the atmosphere and formed Na_2CO_3 under the efflorescence phenomena. Also, the presence of unreacted potassium (in a system with potassium as an activator) under the efflorescence phenomena form potassium carbonate (K_2CO_3) [15].

The tungsten mining waste-based alkali-activated binder (sample prepared with 100 %TMWM and SS+NaOH 8M as activator solutions) was studied in **Paper V**. The TMWM particles were well embedded and connected to the matrix. Some particles are partly covered with needle-like phase. After the alkaline activation, the needles in the 100TM-AAB may correspond to the formation of natrite (Na_2CO_3) needles. The low reactivity of TMWM cause the formation of natrite (Na_2CO_3), were the Na^+ cation in the mixture remained unreacted. During the curing time, the $2Na^+$ reacted with the CO_2^{-3} and formed Na_2CO_3 under the efflorescence phenomena, as shown in equation (2) and (3).

$$CO_{2(g)} + 2OH^-_{(aq)} \rightarrow CO_2^{-3}{}_{(aq)} + H_2O \quad (2)$$

$$2Na^+_{(aq)} + CO_2^{-3}{}_{(aq)} + 7H_2O \rightarrow Na_2CO_3.7H_2O_{(s)} \quad (3)$$

According to Zhang et al [75], this is therefore a partial neutralization for alkaline activation under natural carbonation conditions, as dissolved CO_2 acts as an acid and consumes hydroxides. The main reason for efflorescence in these materials is the availability of mobile Na^+ and OH^-, which remains as unreacted from the alkaline activator solutions.

Although the different type of the alkaline activator used to make the alkaline activation of the TMWM precursor, there were needles in both microstructures of the TMWM-AAB matrix.

The EDS analyses of the TMWM-AAB samples showed that the major elements in the pastes are Silicon (Si), Sodium (Na), Aluminium (Al), and Calcium (Ca). The reaction product of the tungsten mining waste-based alkali-activated mixture had the chemical compositions: Si= 51.74%, Na= 16.4%, Al= 14.0 % and Ca= 13.67%, with Al/Si, Ca/Si and Al/Ca ratios equal to 0.27, 0.26 and 1.03, respectively. These values and ratios indicate the formation of a gel richer in Na and Al and poorer in Ca corresponding to sodium aluminium-silicate hydrate (N-A-S-H) gel. The low Ca/Si ratio exhibited by this gel was consistent with the presence of tetrahedral aluminium (AlO^4) together with sodium ions (Na^+) in the mix; the reaction product phases take up substantial amounts of tetrahedral aluminium in their structure to form (N, C)-A-S-H gel [76].

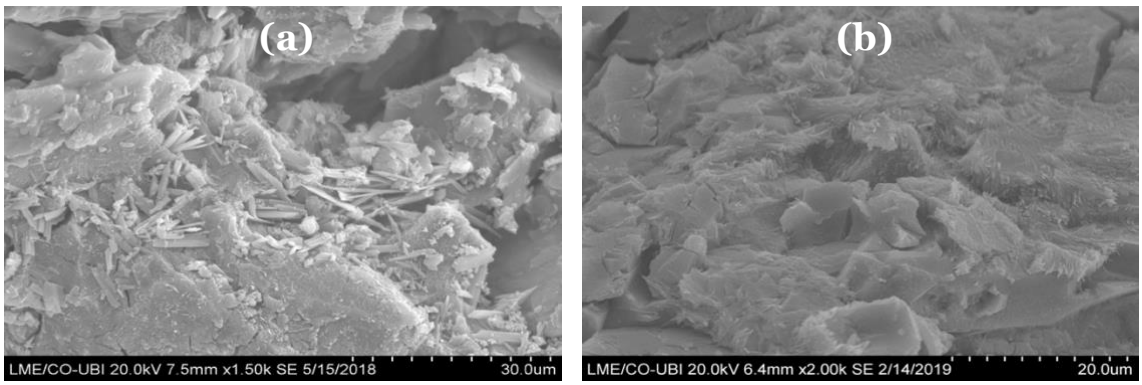

Fig. 9. Scanning electron microscope images of the TMWM-based alkali-activated binder: a)-activated by SS+NaOH 8M; b)-activated by SS+KOH 8M.

4.2.3.2. Microstructure analysis of the blended TMWM with other mineral wastes-based alkali-activated binders

The SEM images of the blended red clay brick waste and tungsten mining waste mud-based alkali-activated binder samples show a matrix with low cohesion/connection between the precursor's particles, due to the partially dissolution of the powder in the alkaline medium. These unreactive particles do not contribute to the compressive strength of the resulting binders. Besides, SEM images present both crystalline and amorphous phases. Some large particles embedded in the matrix indicate that the particle size distribution has the main role in completing the alkaline activation process. However, smaller particles reacted and dissolved during the alkaline activation process [77]. The increase of RCBW in the matrix is offset by the rise in smaller particles that dissolved and produced more reaction product phases. The SEM micrographs of the five AABs prepared in **Paper II**, indicate that the specimens which contained higher dosages of RCBW presented a denser and homogeneous gel when compared with the specimens containing fewer dosages of RCBW. These, in turn,

exhibit low microstructural particle cohesion and lower mechanical strength. The unreacted particles reduced the compressive strength. It can be concluded that microstructural observations are in good accordance with the mechanical properties.

The EDX analysis confirmed the coexistence of unreacted particles surrounded by alkaline activation reaction products. Various phases form as reaction products in the blended AABs, the formation of N-A-S-H and K-A-S-H and the combination (N, K)-A-S-H gels. These reaction product phases possess high ratios of Al/Si, Na/Si, and K/Si with the value of 0.371, 0.124), and 0.173 respectively, and a low Ca/Si ratio of 0.006. Furthermore, phase characterisation becomes more complicated for alkali-activated binders made from precursors (alumina-silicate sources) with some calcium [78]. The formation of K-A-S-H gels due to Al/Si and K/Si ratios and N-A-S-H gels' formation is due to the Al/Si and Na/Si. However, the presence of tetrahedral aluminium (AlO_4) together with sodium ions (Na^+) in the mixes, and with the low Ca/Si content the gels take up substantial amounts of tetrahedral aluminium in their structure to form (N,C)-A-S-H gels in these types of AABs [76]. The presence of calcium and the higher Ca/Si ratio modifies N-A-S-H gels' structure by replacing part of the sodium with calcium to form (N,C)-A-S-H gels [79].

In **Paper III,** the SEM images showed an important structure with a compact and homogeneous morphology. A large proportion of unreacted particles of TMWM and GGBFS grains (inner product) was evident. Moreover, the formation of different types of reaction products (outer products) surrounding the unreacted particles is shown. It is seen that similar types of reaction products are formed in all the binder specimens illustrated from SEM-EDX analysis. The microstructure observation reveals that outer reaction products (N-A-S-H, C-A-S-H, K-A-S-H, and (C, M)-A-S-H gels M = K, Na) and inner reaction products grow successively around the reacting TMWM and GGBFS grains.

The SEM analysis for the AABs prepared with blended EAF-Slag, and TMWM in **Paper IV** showed that the morphology has changed and became denser upon the increase of the EAF-Slag content in the mixtures microstructure due to higher reactivity of the EAF-Slag. In the AABs samples, there was a formation of different reaction products ((N, C)-A-S-H and C-A-S-H phases) with a globular morphology. The increase of the alumina-silicate reaction products in the sample was able to cause an increase in compressive strength. However, the N-A-S-H decreased with the increase of EAF-Slag content in the mixtures. The EAF-Slag alkali-activated binder sample's microstructure shows the presence of some EAF-Slag particles that have not reacted with the alkaline activator solution yet.

Moreover, different microstructures were developed because of the reactive nature of the EAF-Slag. The alkaline activation of EAF-Slag provided a large amount of irregular shape (amorphous) morphology due to C-A-S-H formation and (N, C)-A-S-H. Still, the formation of N-A-S-H was observed in a lower quantity. The EDS results indicated that the Ca:Si and Ca:(Al + Si) ratios were significant to the compressive strength performance of the blended (TMWM + EAF-Slag) alkali-activated specimens. The Ca:Si ratio changed from 0.33 and 1.6 and the Ca:(Al + Si) changed from 0.26 and 1.19 when the EAF-Slag content in the mixtures increased from 10 to 50 vt.%, which revealed that the increase of the Ca:Si and Ca:(Al + Si) ratios resulted in the increasing strength of the binary alkali-activated specimens.

The SEM analyses of the alkali-activated blended ternary precursors (TMWM, GGBFS and MK) was investigated in **Paper V**; it is shown that the microstructure of the ternary AAB was different compared to the sample prepared using 100% TMWM. The matrix formation process in TMWM-AAB is different from that seen in the Ternary-AAB, which results in different reaction products. In the Ternary-AAB sample, the formation of structure gel was observed. In general, three major morphological features were observed, crystalline particles (such as quartz or muscovite or illite) with tabular type particles with no sharp geometric outline (unreacted particles), coated by the reaction product on the surface where it could not be asserted whether in these mixtures coexisted C-A-S-H and N-A-S-H phases or one hybrid (M,C)-A-S-H gel where M is Na or K. The SEM images of the blended binders are shown in Fig. 10 above.

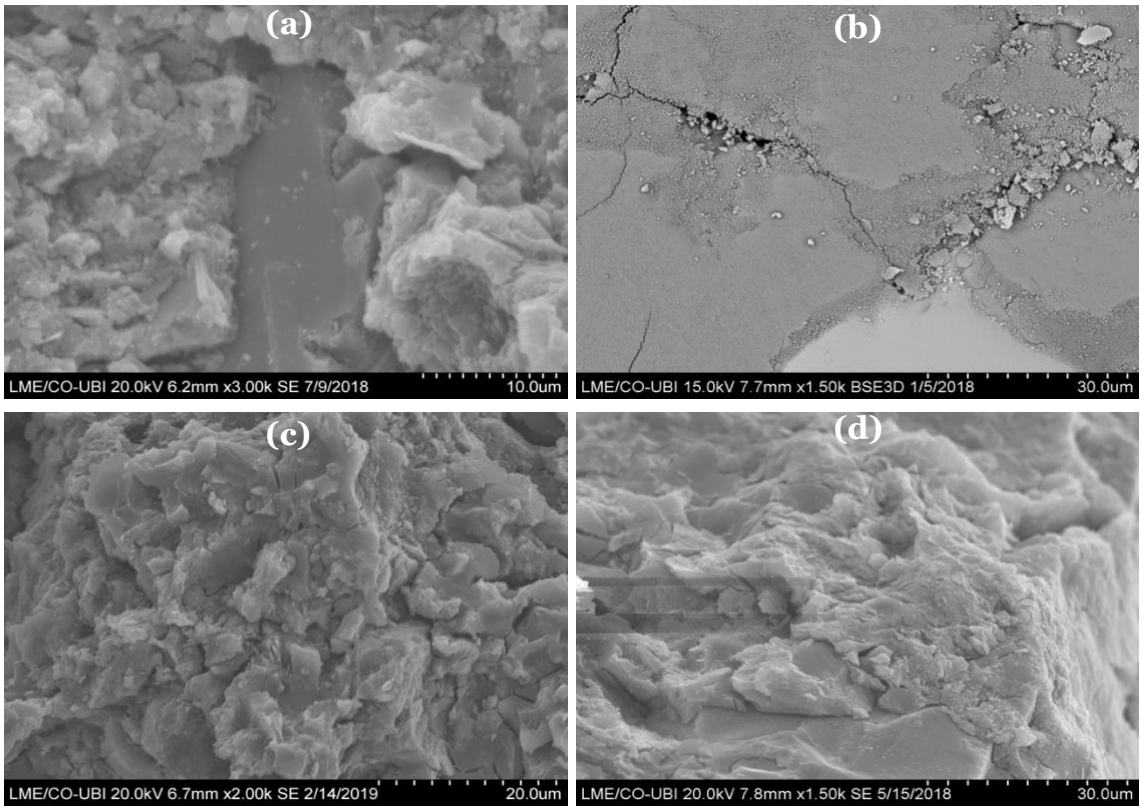

Fig. 10. SEM images of the different blended binders:
(a) TMWM and RCBW; (b)-TMWM and GGBFS; (c) TMWM and EAF-Slag; (d)- TMWM, GGBFS and MK.

4.2.4. X-ray Diffraction analyses of the binders

The XRD analyses were conducted on the binders in **Paper III** and **IV**, to identify the phases that remained unreacted, and the reaction products formed after the alkaline activation process. The unreacted crystalline phases and the alkaline activation reaction products formed in all the binders developed in this research are summarised in Table 15. All the blended binders that were included in this research show that the quartz, muscovite and illite remained as unreactive products, which are the main crystalline phases that constitute the raw TMWM. There were also unreacted crystalline phases from each precursor blended with the TMWM due to the second blended precursor's crystalline nature. The XRD analysis of the blended AABs noticed that similar reaction products were detected in all developed binders such as C-S-H, N-A-S-H, and C-A-S-H gels addition to (N,C)-A-S-H gel. Although the AABs generate the same reaction products, the different reaction products were variate in the matrixes as it is shown in Table 15. The alkali-activated samples that contain more reaction product phases yielded more compressive strength.

Table 15. The main reaction products formed in the different binders after the alkaline activation.

Paper (s)	Binders	Alkaline reaction Products
Paper IV	100TMWM	C-S-H, C-A-S-H, N-A-S-H and (N, C)-A-S-H gels
Paper III	HABs	C-S-H, C-A-S-H, N-A-S-H and (N, C)-A-S-H gels
Paper IV	TMWM+EAF-Slag	C-S-H, C-A-S-H, N-A-S-H and (N, C)-A-S-H gels

4.2.5. Fourier Transform Infra-Red analyses of the binders

Fourier Transforms Infra-Red (FT-IR) spectroscopy tests were carried out to determine the reaction products and their relative intensities according to the measured absorbance in **Papers II, III, IV, V** and **VI**. The recorded spectra of the different binders (tungsten mining waste-based alkali-activated binder and blended binders) are investigated in this research.

The FT-IR spectra of all binders' specimens show a different absorption due to either the precursors' composition, which remained unreacted or the reaction products formed. The shift of the peaks and the bands absorption coefficient depends on the consumption of some compositions and new products' formation. The absorption bands that are shifted from one specimen to another depends on the reaction products formed in the matrix after the alkaline activation. All the binders show main absorbance spectra [(a): Symmetric stretching vibration (Si-O-Si), (b): Asymmetric stretching vibration (T-O-Si, T= Si or Al), (c): Stretching vibration of CO_2, (d): Bound water molecules (H-O-H), (e): Stretching vibration of O-H bond).

The FT-IR spectra of the 100% tungsten mining waste-based alkali-activated binder is investigated in **Paper V**. In addition to the bonds related to unreacted composition and the reaction products, there were important bonds related to the stretching vibration of O-C-O bond at approximately 1450-1410 cm^{-1} indicating the presence of carbonate mineral which has occurred by the atmospheric carbonation, and the coexist of calcite ($CaCO_3$) as unreacted particles from GGBFS. Moreover, the presence of natrite (Na_2CO_3) may due to the carbonation of the large amounts of Na carried to the surface. The TMWM-AAB formed more sodium carbonate due to the unreacted sodium content in the mixture then the unreacted sodium forming sodium carbonate with CO_2 of the atmosphere. Also, a broad band at wavenumber 1436 cm^{-1} appeared only in the TMWM-AAB which corresponded to sodium carbonate Na_2CO_3 (Natrite) [79] and disappeared in the ternary-AAB. The starting materials means that natrite (Na_2CO_3) formed only in TMWM-AAB after the alkaline activation.

In **Papers II** and **IV**, the FT-IR spectra study was about the effect of the different dosages of other mineral wastes in the blended precursor's systems. All the FT-IR spectra showed bands corresponding to the unreacted compositions like quartz, mullite and muscovite from TMWM, and unreacted compositions from RCBW EAF-Slag such as quartz and calcite. However, there was a change in the bands' intensity and the appearance of new bands related to the formation of new components in the blended binder systems. The amorphous alkali-activated structure reaches maximum intensity with the increasing of other mineral wastes (RCBW or EAF-Slag) dosages in the AABs system. The higher intensity corresponds to higher compressive strength. By contrast, the lowest intensity corresponds to a decrease in the compressive strength.

In **Paper III,** the FT-IR analysis was conducted to investigate the effect of the different alkaline activators, the activator's concentration, and the liquid/solid ratios. It showed different bands corresponding to the unreacted composition from TMWM and GGBFS or the reaction products formed after the alkaline activation.

The FT-IR spectra investigated in **Paper V** have shown similar bands to the previously blended binders developed in this research, which had FT-IR bands for unreacted compositions and formation of new alkaline activation products. A special broad band at wavenumber 1436 cm^{-1} appeared only in the blended AAB which corresponded to sodium carbonate Na_2CO_3 (Natrite) and disappeared in the ternary-AAB. The starting materials means that natrite (Na_2CO_3) formed only in 100-TMWM-AAB system. However, the blended AAB that does not show this band means that the natrite is not formed in the blended binders, and all the soluble sodium contained in the activator are reacted with the precursors. Furthermore, in **Paper VI,** the FT-IR analysis showed similar wavenumber bands corresponding to the unreacted composition and the reaction products formed. The intensity of reaction products bands increases with the intensification of compression pressure.

4.2.6. Pore structure of the binders

4.2.6.1. Porosity

The total intruded volume of mercury allows the measurement of the porosity accessible to mercury at maximum applied pressure. Although it has been suggested that the pressure range close to the maximum applied pressure may crush pore walls, the total intruded

volume remains a useful index for comparing pore structure between different mixture designs [80, 81]. The total porosity is the total intruded Hg volume in the sample, and graphically the total porosity represents the maximum value on the intrusion curve [82].

In this research, the porosity of the alkali-activated binders in **Papers II, III** and **IV** was determined by MIP. In **Papers II and IV**, the first observation shows that the partial replacement of TMWM by other mineral waste in the mixtures has a determinant influence on the total porosity. Although the total porosity decreased with the increase of the other mineral wastes dosages in the mixtures, the experimental results show that the total porosity and compressive strength are directly correlated: the higher the binders' compressive strength, the lower the total porosity. Moreover, there is a positive correlation between the total porosity and compressive strength affected by the added mineral waste powder's content in the mixtures. Therefore, the mineral waste powder content increased in the mixtures' offset by lower total porosity in the samples, thus positively affecting and enhancing the blended binders' compressive strength. In **Paper III**, the porosity was affected by the change in the type of the alkaline activator, the activator concentrations, and solid/liquid ratios.

4.2.6.2. Pore-Size distribution

To gain more insight into the pore size distribution of the AABs with the partial replacement of other mineral wastes content in the mixtures, the measured pore distribution is divided into four size ranges according to the International Union of Pure and Applied Chemistry (IUPAC) system [83]. Pores in the cementitious materials can be classified as micropores ($d < 2$ nm), mesopores (2 nm $< d < 50$ nm), macropores (50 nm $< d < 10$ μm) and voids and micro-cracks ($d > 10$ μm). The micropores (ranges $d < 2$ nm) cannot be measured using the MIP technique because the data given is limited and only a minimum pore diameter of 0.005 μm (5 nm) can be evaluated. However, it is possible to measure the mesopores, macropores, and voids and microcrack. It is noticed that the pore ranges change significantly in the samples with a higher content of other mineral wastes (RCBW and EAF-Slag powders) when compared to the original sample containing 100% TMWM.

The pore size distribution of the tungsten mining waste based-alkali-activated binder (100% TMWM as a precursor) activated with potassium hydroxide 8M was studied in **Paper IV**. The dominant range is the range of air voids/cracks (65.44%) followed by macropores (30.89%) and a small range of mesopores (3.67%). However, for the blended binders' samples studied in **Papers II** and **IV**, it was clear that when the content of added dosages

of other mineral wastes in the mixtures increases, the pore size distribution curves shifts to smaller pore sizes, indicating a denser microstructure of the blended AABs samples.

In this research, the effect of the alkaline activators' types, the activators' concentration, and the solid/liquid ratios on the pore size distribution were also investigated in **Paper III**. It was noticed that the pore size distribution was changed and affected by the change in the types of the activator, the activator concentrations, and the liquid/solid ratios.

4.2.6.3. Average pore diameter

The average pore diameter or mean pore diameter was calculated using pore volume and the surface area by the ratio between 4 times the total pore volume and the pore surface area (4V/A). This average value simplifies the real pore structure by a cylindrical tube with its equivalent diameter. The average pore diameter of the different binders was determined in **Papers II, III** and **IV**. It was observed in **Papers II** and **IV** that the average pore diameter decreased proportionally when the content of the other mineral wastes dosages in the mixtures increased. However, the effect of the types of alkaline activator, the concentrations of the alkaline activator, and the solid/liquid ratios on the average pore diameter are discussed in **Paper III**. There is a correlation between the average pore diameter and compressive strength of the blended binders. The compressive strengths tend to increase as the average diameters of pores decreased. According to Moon et al. [84], the average pore diameter significantly influences chloride diffusivity.

4.2.6.4. Critical pore diameter

The pore diameter corresponding to the highest rate of mercury intrusion per change in pressure is known as the characteristic of continuous pore diameter (size), "critical," or "percolation" pore diameter [85–87]. From the Differential Pore Size Distributions (DPSD) curve, the highest point on the corresponding logarithmic differential pore volume curve corresponds to the critical pore (size) diameter. The critical pore (size) diameter was measured at the curve's steepest slope from the cumulative porosity curve. It is considered that all pore sizes refer to the percolation of mercury into the size pore diameter in an interconnected structure. The critical pore diameter provides an index to compare pore structures between different alkali-activated mix designs [82, 88, 89]. Though the critical pore diameter may provide a better indicator of material durability, it has an important influence on the binders' permeability and diffusion characteristics [89, 90]. However, there is no relation between the critical pore diameter and the degree of the alkaline

activation or the related gel/space. The pore structure depends on the quantity of the reaction products formed and how they are packed in the pore space [88].

The study about the critical pore diameter of the blended alkali-activated binders in **Papers II** and **IV** showed that the critical pore diameter gradually decreased with the increase of the mineral wastes' dosages in the blended binder mixtures. The critical pore diameter significantly decreased when TMWM and other mineral wastes are blended, which influences the blended alkali-activated binders' permeability and diffusion characteristics. It is seen that a higher critical pore diameter can be a factor of reduction of compressive strength. In **Paper III** the critical pore diameter showed that the largest fraction of interconnected pores is included in the binder samples prepared with solid/liquid ratio 3, compared to those samples prepared with the solid/liquid ratio 4 that have a greater diameter. Due to the unreacted and evaporated free water, where the water content in the samples prepared with solid/liquid ratio is 3 more than those prepared with solid/liquid ratio 4, the critical pore size does evolve with the increase of solid/liquid ratios.

5. Conclusions and future research

5.1. Conclusions

The mining activity generates millions of tons of solid waste materials during mining's lifetime, disposed of in the open air, which causes several environmental issues during waste management. The mining waste accumulated in large deposits present a potential risk of environmental pollution and cause severe landscape impacts. The low reactivity of tungsten mining waste mud can serve as a favourable waste alumina-silicate source material for synthesising alkali-activated binders, to realise the goal of converting zero value waste materials into valuable construction materials. Although using different alkaline activator solutions to prepare an alkali-activated binder based on tungsten mining waste mud powder as a precursor, a low reactivity during alkaline activation was found in tungsten mining waste mud studied.

Relatively high compressive strength could be obtained by blending tungsten mining waste mud with other mineral wastes (like red clay brick waste, ground granulated blast furnace slag and electric arc furnace slag) and Metakaolin. The blended binders' compressive strengths were further increased by increasing the other mineral wastes content in the composite precursor systems. Higher compressive strengths were obtained when the blended binder systems contained higher dosages of other mineral wastes (50 wt or vt.%). Also, high compressive strength was obtained when replacing 20 wt.% of TMWM with 10 wt.% of GGBFS and 10 wt.% MK in the tungsten mining waste-based alkali-activated binder mixture due to the increase of reactive silicate, aluminium, and calcium content in the mix.

The microstructure analysis (XRD, FT-IR, TG-DTG and SEM-EDS) on the blended binders developed in this research shown the presence of unreacted species such as quartz, muscovite, calcite, and illite from all the raw materials. These analyses also showed the formation of new reaction products due to alkaline activation. After the alkaline activation, the SEM analyses of tungsten mining waste-based alkali-activated binder shown that needles-like phase shape occurred as a reaction product of the fluorescence phenomena. The presence of these needles was identified in the FT-IR spectra as stretching vibration of O-C-O. The formation of needles (natrite) was due to the low reactivity of TMWM, where the Na content in the mixture remained unreacted. During the curing time, the Na reacted with the CO_2 in the atmosphere and formed Na_2CO_3, causing the efflorescence phenomena.

The alkaline activation of the tungsten mining waste-based binder by the alkaline activator solutions formed sodium alumina-silicate hydrates (N-A-S-H) as the main phase due to the presence of the (Si, Al and Na) elements in high content. Also, the formation of (N,C)-A-S-H gel as secondary phase occurred. The formation of this reaction product phases is attributed to the massive amount of available silicate, aluminium, sodium and low content of calcium in the binder admixture. The alkaline activation of the blended precursors with alkaline activator solutions formed different reaction products depending on the second mineral wastes blended with the primary tungsten mining waste mud precursor. C-A-S-H and N-A-S-H gels were formed as main reaction products phases, with C-S-H, K-A-S-H, and (C, M)-A-S-H gels (where M = K, Na) as secondary phases. The amounts of these reaction product phases in the blended binders were depended to the dosages of other mineral wastes content in the blended precursor systems.

The presence of the needles in the tungsten mining waste-based alkali-activated binder sample after the alkaline activation may correspond to the formation of carbonates (such as potassium carbonate (K_2CO_3) and sodium carbonate (Na_2CO_3)). The presence of the needles in the 100TM-AAB after the alkaline activation may correspond to the formation of natrite (Na_2CO_3) needles due to the low reactivity of TMWM. At the same time, the Na content in the mixture remained unreactive. During the curing time, the Na reacted with the CO_2 in the atmosphere and formed Na_2CO_3 under the efflorescence phenomena. Also, the presence of unreacted potassium (in a system with potassium as an activator) under the efflorescence phenomena form potassium carbonate (K_2CO_3). The addition of reactive precursor powders into the tungsten mining waste-based alkali-activated mixtures solve the problem efflorescence phenomena that tungsten mining waste-based alkali-activated binder suffer, which may enhance the durability and avoid further degradation caused by the occurrence of efflorescence's on alkali-activated binders.

The suitability of reusing waste glass powder as an alkaline activator by dissolving waste glass powder in sodium hydroxide is also discussed to have a clear impression on the compressive strength development and the microstructure properties. The dissolving of waste glass powder in sodium hydroxide slightly increased the compressive strength and improved the binders' microstructure properties by forming more reaction products. The dissolved waste glass powder in sodium hydroxide slightly increased the sodium silicate solution SiO_2/Na_2O in the blended binder mixture. The use of dissolved waste glass powder had a positive effect on the critical pore size diameter and reduced the critical pore diameter by 44%. The reduction of the critical pore size diameter was due to reaction product phases formation, which means that more reaction product phases are formed with more silicate

in the dissolved waste glass powder, which was observed using the FT-IR technique. A higher formation of reaction product phases implies an increase in the cohesion between unreacted particles, decreasing the critical pore diameter.

The suitability of using two solid wastes powders (i.e. TMWM and GGBFS) blended with an alumino-silicate source rich material (MK) in alkali-activated binders is investigated. Important physical and chemical properties of the applied GGBFS and MK thoroughly characterised. It is not surprising that the addition of GGBFS and MK are positively affects the compressive strength results and microstructure properties of the blended binder because of the mineralogical nature of GGBFS and MK (amorphous mineralogy) and chemical compositions of MK which is rich in reactive silicate and aluminium and GGBFS rich in silicate and calcium. Clarifying the effect of precursors (GGBFs and MK) on reaction kinetics is necessary since the potential reactivity is highly related to the TMWM. The use of GGBFS and MK into tungsten mining wasted-based alkali-activated binders system shows advantages in sustainable development.

The investigation into the pore structure of binders showed that the pore size distribution of the blended binders matrix reduced as the other mineral wastes content in the blended precursor's systems increased. However, a range of voids/microcracks was found in tungsten mining waste-based alkali-activated binder and blended binders' specimens. It seemed that the range of voids/microcracks reduce as the other mineral wastes content in the blended precursor's systems increased. The average and critical pore diameters also decreased with increasing the other mineral wastes in the blended mixture systems, providing a better indicator of material durability. It has an important influence on the permeability and diffusion characteristics of the blended binder pastes. The decrease of average and critical pore diameters of the blended binders can also affect progressing compressive strength. The research shows that the alkaline activation of the blended TMWM with other minerals waste (alumina-silicate rich materials) is highly beneficial because it increases the AABs' compressive strengths, reduces the porosity and the development of a denser microstructure, which will result in better durability properties.

The intensification of the compression pressures applied on the mixtures made by (50 wt.% TMWM and EAF-Slag) and low liquid to solid ratio in cubic molds, enhances the compressive strength results of the compressed binders. A positive correlation between the compression pressure and the compressive strength gain was found. Using high-pressure loads in producing low liquid to solid blended binder for engineering stone-like materials

from 60 to 100 MPa can efficiently make a valuable binder with superior advantages in low production costs and higher durability.

5.2. Future research

For optimising the production of alkali-activated binders based on tungsten mining waste mud as a sustainable alternative binder to Portland cement, and for developing a deeper and more thorough understanding of the microstructure properties and the compressive strength development of the tungsten mining waste-based alkali-activated binders, there is still several future research that needs to be investigated:

- The use of other mineral wastes as a source of alumino-silicate source materials and alternative alkaline activator solutions might also have the merits of improving the tungsten mining waste-based properties alkali-activated binders. Based on the knowledge obtained from this study, it would be important to emphasise the importance of the mineralogy of the precursors and the chemical compositions of the binder mixtures when investigating different precursors and different alkaline activators.

- It will be valuable to investigate the formation of different types of reaction products formed after the alkaline activation of the precursors using other advanced test methods such as nuclear magnetic resonance (NMR) and XRD (Area Ratio Method (ARM) and Partial or No Known Crystal Structure (PONCKS) methods), in addition to those utilised in this study.

- With the data collected and the alkali-activated binder obtain from this study, a life cycle assessment and leaching of heavy metals should be carried on.

References

1. D. E. Angulo-Ramírez, R. Mejía de Gutiérrez, and F. Puertas, “Alkali-activated Portland blast-furnace slag cement: Mechanical properties and hydration,” *Constr. Build. Mater.*, vol. 140, pp. 119–128, 2017.
2. A. Palomo, M. W. Grutzeck, and M. T. Blanco, "Alkali-activated fly ashes: A cement for the future," *Cem. Concr. Res.*, vol. 29, pp. 1323–1329, 1999.
3. Eurostat, "Waste statistics Main statistical findings -Total waste generation." p. 3, 2016.
4. N. Sedira, J. Castro-Gomes, G. Kastiukas, X. Zhou, and A. Vargas, "A review on mineral waste for chemical-activated binders: mineralogical and chemical characteristics," *Min. Sci.*, vol. 24, pp. 29–58, 2017.
5. J. Kiventerä, I. Lancellotti, M. Catauro, F. D. Poggetto, C. Leonelli, and M. Illikainen, "Alkali activation as new option for gold mine tailings inertization," *J. Clean. Prod.*, vol. 187, pp. 76–84, 2018.
6. J. Kiventerä, L. Golek, J. Yliniemi, V. Ferreira, J. Deja, and M. Illikainen, "Utilisation of sulphidic tailings from gold mine as a raw material in geopolymerization," *Int. J. Miner. Process.*, vol. 149, pp. 104–110, 2016.
7. J. Li, M. Hitch, I. M. Power, and Y. Pan, "Integrated mineral carbonation of ultramafic mine deposits—A review," *Minerals*, vol. 8, no. 4, pp. 1–18, 2018.
8. M. Azadi, M. Edraki, F. Farhang, and J. Ahn, "Opportunities for mineral carbonation in Australia's mining industry," *Sustain.*, vol. 11, no. 5, pp. 1–21, 2019.
9. A. Franco, R. Vieira, and R. Bunting, "The Panasqueira Mine at a Glance," *Tungsten*, vol. 3, no. June, pp. 1–12, 2014.
10. B. Wilson and F. Brian Pyatt, "Bio-availability of tungsten in the vicinity of an abandoned mine in the English Lake District and some potential health implications," *Sci. Total Environ.*, vol. 370, pp. 401–408, 2006.
11. T. Kraus, P. Schramel, K. H. Schaller, P. Zöbelein, A. Weber, and J. Angerer, "Exposure assessment in the hard metal manufacturing industry with special regard to tungsten and its compounds," *Occup. Environ. Med.*, pp. 631–634, 2001.
12. J. P. Castro-Gomes, A. P. Silva, R. P. Cano, J. Durán Suarez, and A. Albuquerque, "Potential for reuse of tungsten mining waste-rock in technical-artistic value added products," *J. Clean. Prod.*, vol. 25, pp. 34–41, 2012.
13. F. Pacheco-Torgal, J. Castro-Gomes, and S. Jalali, "Tungsten mine waste geopolymeric binder: Preliminary hydration products investigations," *Constr. Build. Mater.*, vol. 23, pp. 200–209, Jan. 2009.
14. L. Vickers, A. van Riessen, and W. D. a. Rickard, "Precursors and Additives for

Geopolymer Synthesis," in *Fire-Resistant Geopolymers. Springer*, Singapore, 2015, pp. 99–110.

15. M. A. Longhi, Z. Zhang, E. D. Rodríguez, A. P. Kirchheim, and H. Wang, "Efflorescence of alkali-activated cements (geopolymers) and the impacts on material structures: A critical analysis," *Front. Mater.*, vol. 6, no. April, pp. 1–13, 2019.
16. H. Jones and D. V. Boger, "Sustainability and Waste Management in the Resource Industries," *Ind. Eng. Chem. Res.*, vol. 51, no. 30, pp. 10057–10065, 2012.
17. I. Silva, J. P. Castro-Gomes, and A. Albuquerque, "Effect of immersion in water partially alkali-activated materials obtained of tungsten mine waste mud," *Constr. Build. Mater.*, vol. 35, pp. 117–124, Oct. 2012.
18. J. Kiventerä, P. Perumal, J. Yliniemi, and M. Illikainen, "Mine tailings as a raw material in alkali activation : A review," vol. 27, no. 8, 2020.
19. J. Rivera, F. Castro, A. Fernández, and J. Nuno, "Alkali - Activated Cements from Urban , Mining and Agro - Industrial Waste : State - of - the - art and Opportunities," *Waste and Biomass Valorisation*, no. 0123456789, 2020.
20. F. Demir and E. M. Derun, "Modelling and optimisation of gold mine tailings based geopolymer by using response surface method and its application in Pb 2 þ removal," *J. Clean. Prod.*, vol. 237, p. 117766, 2019.
21. F. Pacheco-Torgal, J. P. Castro-Games, and S. Jalali, "Alkali activated geopolymeric binder using Tungsten mine waste: preliminary investigation," *Geopolymer, Green Chem. Sustain. Dev. Solut.*, pp. 93–98, 2005.
22. G. Kastiukas, D. Ph, X. Zhou, D. Ph, M. Asce, and J. Castro-gomes, "Preparation Conditions for the Synthesis of Alkali-Activated Binders Using Tungsten Mining Waste," *J. Mater. Civ. Eng.*, vol. 29, no. 10, pp. 1–9, 2017.
23. G. Kastiukas and X. Zhou, "Effects of waste glass on alkali-activated tungsten mining waste: composition and mechanical properties," *Mater. Struct. Constr.*, vol. 50, no. 4, 2017.
24. T. Luukkonen, Z. Abdollahnejad, J. Yliniemi, P. Kinnunen, and M. Illikainen, "One-part alkali-activated materials: A review," *Cem. Concr. Res.*, vol. 103, no. July 2017, pp. 21–34, 2018.
25. L. Gomez-Zamorano, M. Balonis, B. Erdemli, N. Neithalath, and G. Sant, "C–(N)–S–H and N–A–S–H gels: Compositions and solubility data at 25°C and 50°C," *J. Am. Ceram. Soc.*, vol. 100, no. 6, pp. 2700–2711, 2017.
26. H. Kühl, "Slag Cement and Process of Making the Same," 1908.
27. A.O. Purdon, "The action of alkalis on blast-furnace slag," *J. Chem. Soc. Chem. Commun.*, vol. 59, pp. 191–202, 1940.

28. A. Buchwald, M. Vanooteghem, E. Gruyaert, H. Hilbig, and N. De Belie, "Purdocement: application of alkali-activated slag cement in Belgium in the 1950s," *Mater. Struct. Constr.*, vol. 48, no. 1–2, pp. 501–511, 2015.
29. C. Shi, P. Krivenko, and D. Roy, *Activated Cements and Concretes*. Taylor & Francis, 2006.
30. J. I. Escalante García, K. Campos-Venegas, A. Gorokhovsky, and A. Fernández, "Cementitious composites of pulverised fuel ash and blast furnace slag activated by sodium silicate: Effect of Na2O concentration and modulus," *Adv. Appl. Ceram.*, vol. 105, no. 4, pp. 201–208, 2006.
31. C. K. Yip, G. C. Lukey, and J. S. J. Van Deventer, "The coexistence of geopolymeric gel and calcium silicate hydrate at the early stage of alkaline activation," *Cem. Concr. Res.*, vol. 35, no. 9, pp. 1688–1697, 2005.
32. I. García Lodeiro, A. Fernández-Jimenez, A. Palomo, and D. E. Macphee, "Effect on fresh C-S-H gels of the simultaneous addition of alkali and aluminium," *Cem. Concr. Res.*, vol. 40, no. 1, pp. 27–32, 2010.
33. I. G. Lodeiro, D. E. Macphee, A. Palomo, and A. Fernández-jiménez, "Effect of alkalis on fresh C – S – H gels . FTIR analysis," *Cem. Concr. Res.*, vol. 39, no. 3, pp. 147–153, 2009.
34. I. Ismail, S. A. Bernal, J. L. Provis, R. San Nicolas, S. Hamdan, and J. S. J. Van Deventer, "Modification of phase evolution in alkali-activated blast furnace slag by the incorporation of fly ash," *Cem. Concr. Compos.*, vol. 45, pp. 125–135, 2014.
35. J. L. Provis, "Geopolymers and other alkali activated materials: Why, how, and what?," *Mater. Struct. Constr.*, vol. 47, no. 1–2, pp. 11–25, 2014.
36. N. R. Rakhimova and R. Z. Rakhimov, "Reaction products, structure and properties of alkali-activated metakaolin cements incorporated with supplementary materials - A review," *J. Mater. Res. Technol.*, vol. 8, no. 1, pp. 1522–1531, 2019.
37. N. R. Rakhimova and R. Z. Rakhimov, "Alkali-activated cements and mortars based on blast furnace slag and red clay brick waste," *Mater. Des.*, vol. 85, pp. 324–331, 2015.
38. C. Li, J. Wan, H. Sun, and L. Li, "Investigation on the activation of coal gangue by a new compound method," *J. Hazard. Mater.*, vol. 179, pp. 515–520, 2010.
39. J. He, Y. Jie, J. Zhang, Y. Yu, and G. Zhang, "Synthesis and characterisation of red mud and rice husk ash-based geopolymer composites," *Cem. Concr. Compos.*, vol. 37, pp. 108–118, Mar. 2013.
40. D. H. Francis A. Kuranchie, Sanjay K. Shukla, "Utilisation of iron ore mine tailings for the production of geopolymer bricks," *Int. J. Mining, Reclam. Environ.*, vol. 30, no. 2, pp. 92–114, 2014.

41. A. R. Mwesigye, S. D. Young, E. H. Bailey, and S. B. Tumwebaze, "Population exposure to trace elements in the Kilembe copper mine area, Western Uganda: A pilot study," *Sci. Total Environ.*, vol. 573, pp. 366–375, 2016.
42. F. Pacheco-Torgal, J. P. Castro-Gomes, and S. Jalali, "Adhesion characterisation of tungsten mine waste geopolymeric binder. Influence of OPC concrete substrate surface treatment," *Constr. Build. Mater.*, vol. 22, pp. 154–161, Mar. 2008.
43. T. Sun, J. Chen, X. Lei, and C. Zhou, "Detoxification and immobilisation of chromite ore processing residue with metakaolin-based geopolymer," *J. Environ. Chem. Eng.*, vol. 2, pp. 304–309, 2014.
44. X. Jiao, Y. Zhang, and T. Chen, "Thermal stability of a silica-rich vanadium tailing based geopolymer," *Constr. Build. Mater.*, vol. 38, pp. 43–47, 2013.
45. M. H. Wu, C. L. Lin, W. C. Huang, and J. W. Chen, "Characteristics of pervious concrete using incineration bottom ash in place of sandstone graded material," *Constr. Build. Mater.*, vol. 111, pp. 618–624, 2016.
46. R. Siddique, *Waste materials and by-products in concrete*. 2008.
47. E. Khankhaje, M. W. Hussin, J. Mirza, M. Rafieizonooz, M. R. Salim, H. C. Siong, M. Warid., "On blended cement and geopolymer concretes containing palm oil fuel ash," *Mater. Des.*, vol. 89, pp. 385–398, 2016.
48. M. Jeguirim, L. Limousy, and P. Dutournie, "Pyrolysis kinetics and physicochemical properties of agropellets produced from spent ground coffee blended with conventional biomass," *Chem. Eng. Res. Des.*, vol. 92, no. 10, pp. 1876–1882, 2014.
49. S. Yan and K. Sagoe-Crentsil, "Properties of wastepaper sludge in geopolymer mortars for masonry applications," *J. Environ. Manage.*, vol. 112, pp. 27–32, 2012.
50. E. Nimwinya, W. Arjharn, S. Horpibulsuk, T. Phoo-Ngernkham, and A. Poowancum, "A sustainable calcined water treatment sludge and rice husk ash geopolymer," *J. Clean. Prod.*, vol. 119, pp. 128–134, 2016.
51. J. Yliniemi, P. Kinnunen, P. Karinkanta, and M. Illikainen, "Utilisation of Mineral Wools as Alkali-Activated Material Precursor," *Materials (Basel).*, vol. 9, no. 5, p. 312, 2016.
52. E. D. Rodriguez, S. A. Bernal, J. L. Provis, J.D. Gehman, J. M. Monzi, J. Payi, M.V. Borrachero., "Geopolymers based on spent catalyst residue from a fluid catalytic cracking (FCC) process," *Fuel*, vol. 109, pp. 493–502, 2013.
53. A. Nazari, A. Bagherim, and S. Riahi, "Properties of geopolymer with seeded fly ash and rice husk bark ash," *Mater. Sci. Eng. A*, vol. 528, pp. 7395–7401, 2011.
54. M. Frias, M. I. Sánchez De Rojas, J. Santamaría, and C. Rodríguez, "Recycling of silicomanganese slag as pozzolanic material in Portland cements: Basic and engineering properties," *Cem. Concr. Res.*, vol. 36, pp. 487–491, 2006.

55. D. Stock, "World production and consumption of ceramic tiles," 2014.
56. P. Perumal, K. Piekkari, H. Sreenivasan, and P. Kinnunen, "One-part geopolymers from mining residues – Effect of thermal treatment on three different tailings," *Miner. Eng.*, vol. 144, no. February, p. 106026, 2019.
57. H. Paiva, J. Yliniemi, M. Illikainen, F. Rocha, and V. M. Ferreira, "Mine Tailings Geopolymers as a Waste Management Solution for A More Sustainable Habitat," *sustainability*, vol. 11, no. 995, 2019.
58. J. Xiangke, Z. Yimin, C. Tiejun, B. Shenxu, L. Tao, and H. Jing, "Geopolymerisation of a silica-rich tailing," *Miner. Eng.*, vol. 24, no. 15, pp. 1710–1712, 2011.
59. L. Reig, M. M. Tashima, L. Soriano, M. V. Borrachero, J. Monzó, and J. Payá, "Alkaline activation of ceramic waste materials," *Waste and Biomass Valorization*, vol. 4, pp. 729–736, 2013.
60. S. A. Bernal, E. D. Rodriguez, R. Mejia De Gutiérrez, J. L. Provis, and S. Delvasto, "Activation of metakaolin/slag blends using alkaline solutions based on chemically modified silica fume and rice husk ash," *Waste and Biomass Valorisation*, vol. 3, no. 1, pp. 99–108, 2012.
61. M. M. Khater, "Influence of electric arc furnace slag on characterisation of the produced geopolymer composites," *Epa. - J. Silic. Based Compos. Mater.*, vol. 67, no. 3, p. 2015, 2015.
62. J. J. Chang, "A study on the setting characteristics of sodium silicate-activated slag pastes," *Cem. Concr. Res.*, vol. 33, pp. 1005–1011, 2003.
63. S. Ahmad, Y. Iqbal, and F. Ghani, "Phase and Microstructure of Brick-Clay Soil and Fired Clay-Bricks From Some Areas in Peshawar Pakistan," *J. Pakistan Mater. Soc.*, vol. 2, pp. 33–39, 2008.
64. I. Z. Yildirim and M. Prezzi, "Chemical, mineralogical, and morphological properties of steel slag," *Adv. Civ. Eng.*, vol. 2011, 2011.
65. M. Zhang, S. Redfern, E. Salje, and C. Hayward, "Thermal behavior of vibrational phonons and hydroxyls of muscovite in dehydroxylation : In situ high-temperature infrared spectroscopic investigations," *Am. Mineral.*, vol. 95, 2010.
66. R. P. Orosco, M. C. Ruiz, L. I. Barbosa, and J. A. González, "Purification of talcs by chlorination and leaching," *Int. J. Miner. Process.*, vol. 101, pp. 116–120, 2011.
67. N. Sedira, J. Castro-Gomes, and M. Magrinho, "Red clay brick and tungsten mining waste-based alkali-activated binder: Microstructural and mechanical properties," *Constr. Build. Mater.*, vol. 190, pp. 1034–1048, Nov. 2018.
68. M. Sutcu, "Influence of expanded vermiculite on physical properties and thermal conductivity of clay bricks," *Ceram. Int.*, vol. 41, no. 2, pp. 2819–2827, 2015.
69. A. J. Ajala and N. A. Badarulzaman, "Thermal Conductivity of Aloji Fireclay as

Refractory Material," *Int. J. Integr. Eng.*, vol. 8, no. 3, pp. 16–20, 2016.

70. L. Reig, M. M. Tashima, M. V. Borrachero, J. Monzó, C. R. Cheeseman, and J. Payá, "Properties and microstructure of alkali-activated red clay brick waste," *Constr. Build. Mater.*, vol. 43, pp. 98–106, 2013.
71. B. H. A. Ahmad, Z.A., Johari, I., Said, S., Jaya, R.P., Bakar, "Chemical and Physical Properties of Fired-Clay Brick At Different Type of Rice Husk Ash," *2011 Int. Conf. Environ. Sci. Eng.*, vol. 8, pp. 171–174, 2011.
72. G. Ya-min, F. Yong-hao, Y. Duo, G. Yong-fan, and Z. Chen-hui, "Properties and microstructure of alkali-activated slag cement cured at below- And about-normal temperature," *Constr. Build. Mater.*, vol. 79, pp. 1–8, 2015.
73. H. Song, Y. Jeong, S. Bae, Y. Jun, S. Yoon, and J. Eun Oh, "A study of thermal decomposition of phases in cementitious systems using HT-XRD and TG," *Constr. Build. Mater.*, vol. 169, pp. 648–661, 2018.
74. S. A. Bernal, M. C. Juenger, X. Ke, W. Matthes, B. Lothenbach, N. De Belie, J. L. Provis., "Characterisation of supplementary cementitious materials by thermal analysis," *Mater. Struct. Constr.*, vol. 50, no. 1, pp. 1–13, 2017.
75. Z. Zhang, J. L. Provis, A. Reid, and H. Wang, "Fly ash-based geopolymers: The relationship between composition, pore structure and efflorescence," *Cem. Concr. Res.*, vol. 64, pp. 30–41, 2014.
76. A. Fernandez-Jimenez, E. Flores, O. Maltseva, I. Garcia-Lodeiro, and A. Palomo, "Hybrid Alkaline Cements. Part III. Durability and Industrial Applications," *Rev. Rom. Mater. J. Mater.*, vol. 43, no. 2, pp. 195–200, 2013.
77. M. F. Zawrah, R. A. Gado, N. Feltin, S. Ducourtieux, and L. Devoille, "Recycling and utilisation assessment of waste fired clay bricks (Grog) with granulated blast-furnace slag for geopolymer production," *Process Saf. Environ. Prot.*, vol. 103, pp. 237–251, 2016.
78. S. Puligilla and P. Mondal, "Coexistence of aluminosilicate and calcium silicate gel characterised through selective dissolution and FTIR spectral subtraction," *Cem. Concr. Res.*, vol. 70, pp. 39–49, 2015.
79. L. Reig, L. Soriano, M. V. Borrachero, J. Monzó, and J. Payá, "Influence of calcium aluminate cement (CAC) on alkaline activation of red clay brick waste (RCBW)," *Cem. Concr. Compos.*, vol. 65, pp. 177–185, 2016.
80. R. F. Feldman, "Pore Structure Damage in Blended Cements Caused by Mercury Intrusion," *J. Am. Ceram. Soc.*, vol. 67, no. 1, pp. 30–33, 1984.
81. S. Wild, "A discussion of the paper 'mercury porosimetry - An inappropriate method for the measurement of pore size distributions in cement-based materials' by S. Diamond," *Cem. Concr. Res.*, vol. 31, no. 11, pp. 1653–1654, 2001.

82. D. K. Panesar and J. Francis, "Influence of limestone and slag on the pore structure of cement paste based on mercury intrusion porosimetry and water vapour sorption measurements," *Constr. Build. Mater.*, vol. 52, pp. 52–58, 2014.
83. IUPAC, "Manual of symbols and terminology, appendix 2, part 1, Colloid and Surface Chemistry," *Pure Appl. Chem.*, vol. 31, 1972.
84. H. Y. Moon, H. S. Kim, and D. S. Choi, "Relationship between average pore diameter and chloride diffusivity in various concretes," *Constr. Build. Mater.*, vol. 20, no. 9, pp. 725–732, 2006.
85. R. A. Cook and K. C. Hover, "Mercury porosimetry of hardened cement pastes," *Cem. Concr. Res.*, vol. 29, no. 6, pp. 933–943, 1999.
86. H. Ma, "Mercury intrusion porosimetry in concrete technology: Tips in measurement, pore structure parameter acquisition and application," *J. Porous Mater.*, vol. 21, no. 2, pp. 207–215, 2014.
87. Kalliopi K. Aligizaki, *Pore structure of Cement-Based Materials: Testing, Interpretation and Requirements*. London: Taylor & Francis Group, 2006.
88. Q. Zeng, K. Li, T. Fen-Chong, and P. Dangla, "Pore structure characterisation of cement pastes blended with high-volume fly-ash," *Cem. Concr. Res.*, vol. 42, no. 1, pp. 194–204, 2012.
89. P. Halamickova, R. J. Detwilera, D. P. Bentz, and E. J. Garboczi, "Water permeability and chloride ion diffusion in Portland cement mortars: relationship to sand content and critical pore diameter," *Cem. Concr. Res.*, vol. 25, no. 4, pp. 790–802, 1995.
90. E. J. Garboczi, "Permeability, diffusivity, and microstructural parameters: a critical review," *Cem. Concr. Res.*, vol. 20, pp. 591–601, 1990.
91. EN 196-6:2019 - Methods of testing cement - Part 6: Determination of fineness.

Original publications

I. N. Sedira, J. Castro-Gomes, G. Kastiukas, X. Zhou, and A. Vargas, "A review on mineral waste for chemical-activated binders: mineralogical and chemical characteristics," Mining Science., vol. 24, pp. 29–58, 2017. Available from: doi: 10.5277/msc172402

II. N. Sedira, J. Castro-Gomes, and M. Magrinho, "Red clay brick and tungsten mining waste-based alkali-activated binder: Microstructural and mechanical properties," Construction and Building Materials., vol. 190, pp. 1034–1048, 2018. Available from: https://doi.org/10.1016/j.conbuildmat.2018.09.153

III. N. Sedira and J. Castro-gomes, "Effect of activators on hybrid alkaline binder based on tungsten mining waste and ground granulated blast furnace slag," Construction and Building Materials., vol. 232, p. 117176, 2020. Available from: https://doi.org/10.1016/j.conbuildmat.2019.117176

IV. N. Sedira and J. Castro-Gomes, "Alkali-Activated Binders Based on Tungsten Mining Waste and Electric-Arc-Furnace Slag: Compressive Strength and Microstructure Properties," CivilEng, vol. 1, no. 2, pp. 154–180, 2020. Available from: doi:10.3390/civileng1020010

V. N. Sedira and J. Castro-gomes, "Microstructure Features of Ternary Alkali-activated Binder Based on Tungsten Mining Waste, Slag and Metakaolin," KnE Engineering., vol. 5, no. 4, pp. 195–206, 2020. Available from: DOI 10.18502/keg.v5i4.6810

VI. N. Sedira and J. Castro-Gomes, "Low Liquid-to-solid Ratio of Mining Waste and Slag Binary Alkali-activated Material," KnE Engineering., vol. 2020, pp. 202–213, 2020. Available from: DOI 10.18502/keg.v5i5.6941

Original publications are not included in the electronic version of the thesis.